12. SITE 1018[1]

Shipboard Scientific Party[2]

HOLE 1018A

Date occupied: 22 May 1996

Date departed: 25 May 1996

Time on hole: 3 days, 6 hr, 15 min

Position: 36°59.300′N, 123°16.653′W

Drill pipe measurement from rig floor to seafloor (m): 2488.6

Distance between rig floor and sea level (m): 11.2

Water depth (drill pipe measurement from sea level, m): 2477.4

Total depth (from rig floor, m): 2914.8

Penetration (m): 426.9

Number of cores (including cores having no recovery): 45

Total length of cored section (m): 426.2

Total core recovered (m): 426.9

Core recovery (%): 100

Oldest sediment cored:
Depth (mbsf): 426.2
Nature: Clay with silt, nannofossil chalk with clay
Age: early Pliocene

Comments: Camera survey of the ocean floor was conducted before spudding.

HOLE 1018B

Date occupied: 25 May 1996

Date departed: 25 May 1996

Time on hole: 2 hr

Position: 36°59.380′N, 123°16.532′W

Drill pipe measurement from rig floor to seafloor (m): 2486.8

Distance between rig floor and sea level (m): 11.2

Water depth (drill pipe measurement from sea level, m): 2475.6

Total depth (from rig floor, m): 2506.0

Penetration (m): 19.2

Number of cores (including cores having no recovery): 2

Total length of cored section (m): 19.2

Total core recovered (m): 19.5

Core recovery (%): 101.0

Oldest sediment cored:
Depth (mbsf): 19.2
Nature: Clay with diatoms and silt
Age: Quaternary

Comments: Overshot the mudline.

HOLE 1018C

Date occupied: 26 May 1996

Date departed: 26 May 1996

Time on hole: 23 hr, 30 min

Position: 36°59.388′N, 123°16.538′W

Drill pipe measurement from rig floor to seafloor (m): 2488.0

Distance between rig floor and sea level (m): 11.2

Water depth (drill pipe measurement from sea level, m): 2476.8

Total depth (from rig floor, m): 2750.2

Penetration (m): 262.2

Number of cores (including cores having no recovery): 28

Total length of cored section (m): 262.2

Total core recovered (m): 261.7

Core recovery (%): 99.0

Oldest sediment cored:
Depth (mbsf): 262.2
Nature: Clayey nannofossil ooze with diatoms, clay with silt
Age: late Pliocene

HOLE 1018D

Date occupied: 26 May 1996

Date departed: 27 May 1996

Time on hole: 17 hr, 30 min

Position: 36°59.392′N, 123°16.544′W

Drill pipe measurement from rig floor to seafloor (m): 2487.2

Distance between rig floor and sea level (m): 11.2

Water depth (drill pipe measurement from sea level, m): 2476.0

Total depth (from rig floor, m): 2654.9

Penetration (m): 167.7

Number of cores (including cores having no recovery): 18

Total length of cored section (m): 167.7

Total core recovered (m): 167.4

Core recovery (%): 99.0

Oldest sediment cored:
Depth (mbsf): 167.7
Nature: Clay with silt
Age: Quaternary

Principal results: Site 1018 is located about 75 km west of Santa Cruz, California, on a sediment drift just south of Guide Seamount at a water depth

[1]Lyle, M., Koizumi, I., Richter, C., et al., 1997. *Proc. ODP, Init. Repts.*, 167: College Station, TX (Ocean Drilling Program).

[2]Shipboard Scientific Party is given in the list preceding the Table of Contents.

of 2477 mbsl. The primary objectives at this site were to sample a high-resolution upper Miocene to Holocene sediment section from the central California Margin to study the evolution of the California Current as well as the history of upwelling and productivity. It provides continuity between the Gorda Transect at 40°N and the southern California transects. The site also will be used to collect new data on organic carbon diagenesis and minor element geochemistry through pore-water profiles and solid phase analyses. Organic carbon contents and terrestrial organic matter input are moderately high.

Four holes were cored with the APC/XCB at Site 1018 to a maximum depth of 426.2 mbsf, recovering an apparently continuous interval of Quaternary to uppermost lower Pliocene (0–3.5 Ma) sediments (Fig. 1). Hole 1018A was cored with the APC to 90.4 mbsf and extended with the XCB to 426.2 mbsf. The hole was logged with the density-porosity combination tool string (density, neutron porosity, resistivity, and natural gamma ray) from 225 to 80 mbsf. Two cores were taken with the APC at Hole 1018B down to 19.2 mbsf. Hole 1018C was cored with the APC to 88.5 mbsf and deepened with the XCB to 262.2 mbsf. Hole 1018D was cored with the APC to 104.3 mbsf and extended with the XCB to 167.7 mbsf.

The sedimentary section begins with ~200 m of siliciclastic sediments composed mainly of clays with varied and increasing amounts of diatoms and nannofossils of Quaternary to late Pliocene age (Fig. 1). Thin feldspar quartz sand layers occur frequently in the upper part of the cored sequence. Diatom clay and diatom ooze dominate the middle 145 m of this sequence. The lowest unit (80 m thick) is characterized by clayey nannofossil chalk and nannofossil clay with decreased diatom content. This unit is early to late Pliocene in age. Vitric volcanic ash layers are rare except in the lowermost part of the sequence. Sedimentation rates range between 100 and 200 m/m.y. with an average of 130 m/m.y.

Detailed comparisons between the magnetic susceptibility and the GRAPE density record generated on the MST, and high-resolution color reflectance measured with the Oregon State University system, demonstrated complete recovery of the sedimentary sequence down to 193 mcd.

A well-constrained biostratigraphy and chronology are provided by a combination of calcareous nannofossil, planktonic foraminifer, radiolarian, and diatom datums for the latest early Pliocene and Quaternary. All microfossil groups are dominated by cool, high-latitude elements throughout the late Neogene. Site 1018 is sufficiently far north in the California Current to exclude most to all subtropical species, even during interglacial episodes. Radiolarians are entirely represented by subarctic forms. Diatoms are dominated by subarctic forms with the addition of much less abundant temperate elements. Planktonic foraminifer assemblages are dominated by subarctic to cool temperate forms, with subtropical elements absent except during warmest interglacial episodes. Planktonic foraminifers exhibit glacial to interglacial oscillations throughout. Radiolarians do not exhibit such changes because they chiefly live in deeper water. Changes in microfossil assemblages provide evidence of progressive cooling during the late Neogene. Diatoms are dominated by oceanic forms but during the Quaternary include a small but distinct littoral assemblage that typically lives on sea grass. These forms were reworked from shallow waters and appear to be most abundant during the times of higher input of terrigenous sediments.

Positive paleomagnetic inclinations in the top 88 mbsf most likely represent the Brunhes Chron. Below the normal polarity interval, an interpretation of the inclination record was not possible because of the low magnetic intensity and core disturbance by XCB coring.

Calcium carbonate content is low, ranging between 0 and 5 wt% with frequent spikes up to 17 wt% in the upper 350 mbsf; values increase to 5–25 wt% below that depth. Total organic carbon is mainly of marine origin and has an average concentration of 1.2 wt%. Chemical gradients in the interstitial waters reflect organic matter diagenesis, the dissolution of biogenic opal and calcium carbonate, the influence of authigenic mineral precipitation reactions, and the diffusive influence of reactions in underlying basalt.

In situ temperature measurements at Site 1018 gave a thermal gradient of 32°C/km. Using an average measured thermal conductivity of 0.847 W/(m·K) yields a heat-flow estimate of 27 mW/m^2.

BACKGROUND AND OBJECTIVES

General Description

Site 1018 is located ~75 km west of Santa Cruz, California on a sediment drift just south of Guide Seamount (Figs. 2, 3) in a water depth of 2477 mbsl. Guide Seamount is believed to be a fossil spreading axis that went extinct during magnetic Anomaly 6 (20 Ma; Bohannon and Parsons, 1995; Atwater and Severinghaus, 1989) so the ocean crust beneath Site 1018 should be slightly older than the seamount. The site is located near two abandoned munitions dumps (Fig. 4), which are ~9 km away from the optimal drill site location.

Site 1018 is on top of a sediment mound that rises more than 400 m above its surroundings. The mound's position immediately adjacent to Guide Seamount makes it likely that it is a sediment drift. The Monterey Submarine Canyon and Fan are 50–100 km south, but the most likely proximal source of sediments is to the north from Pioneer Canyon, due west of San Francisco Bay. The seismic reflection profile from the EW9504 survey (Lyle et al., 1995a, 1995b; Fig. 5) shows a thick sediment sequence perhaps 1130 ms TWT thick (~950 m.). The upper part of the sequence is strongly layered to ~180 ms TWT, or 140–150 mbsf, while the middle sequence is more acoustically transparent. Strong acoustic reflectors reappear at ~700 ms TWT below the seafloor, or about 560 mbsf. Drilling terminated within the middle unit.

Site Objectives

At Site 1018 we drilled a high-resolution, lower Pliocene to Holocene sediment section from the central California Margin to study the evolution of the California Current as well as the history of upwelling and productivity. It provides continuity between the Gorda Transect at 40°N and the southern California transects. The site will also gauge the evolution of midwaters during the time in which Northern Hemisphere glaciation developed.

Site 1018 will be used to collect new data on organic carbon diagenesis and about minor element geochemistry through interstitial water profiles and through solid phase analyses. Organic carbon content averages 1.3%, and terrestrial organic matter input may be high. Interstitial water sampling, especially within the upper 100 m, will be used to define organic matter diagenesis, while organic geochemical analysis will provide data on organic matter preservation underneath a well-oxygenated water column.

OPERATIONS

Transit from Site 1017 to Site 1018

The 180.0-nmi transit from Site 1017 to Site 1018 was accomplished in 18.5 hr at an average speed of 9.7 kt. A 3.5-kHz precision depth recorder survey was performed while approaching Site 1018. The *JOIDES Resolution* arrived at Site 1018 at 0815 hr on 22 May.

Hole 1018A

Site 1018 is located approximately 6 nmi outside of an area marked "Explosive Dumping Area Disused." A subsea camera survey of the seafloor was conducted within a 50-m perimeter of the coordinates for Site 1018. One object with the approximate size and shape of a 55-gallon drum was found ~50 m south of Site 1018. The

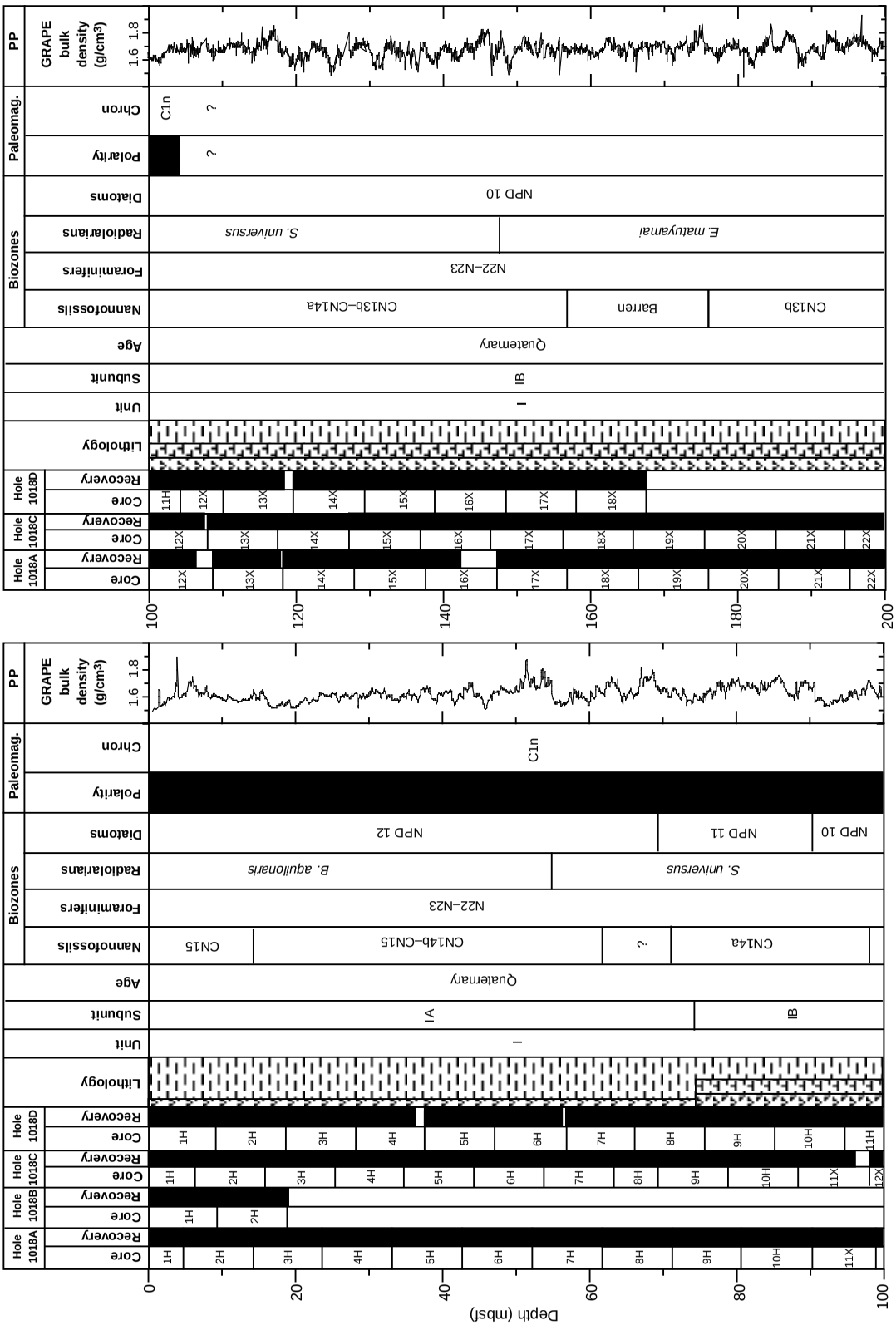

Figure 1. Site 1018 master column.

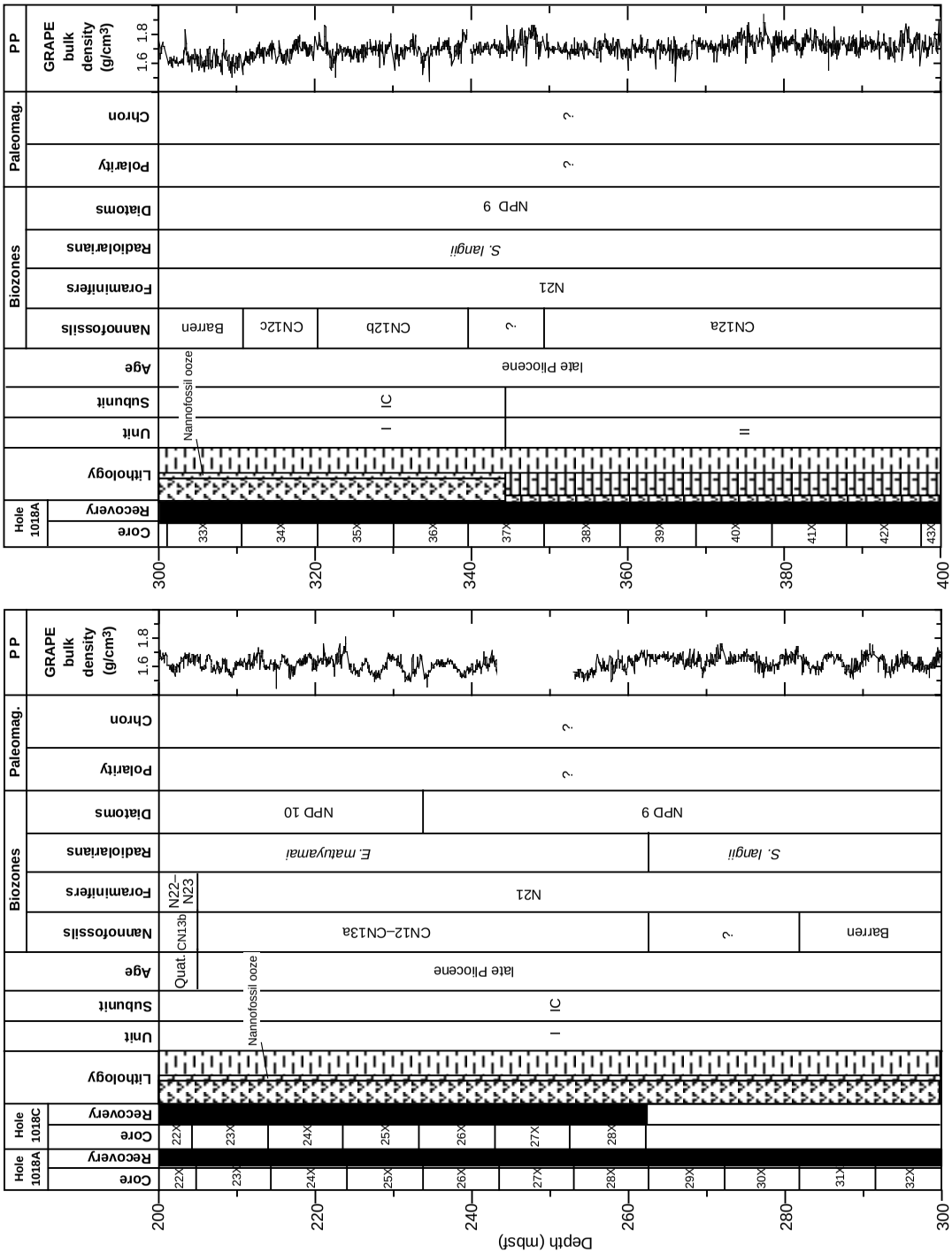

Figure 1 (continued).

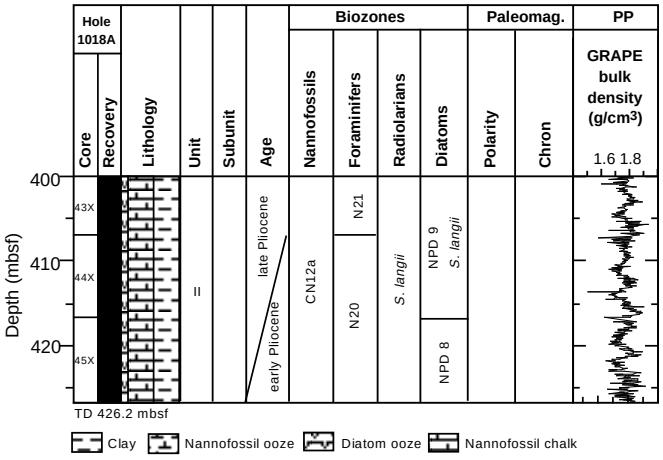

Figure 1 (continued).

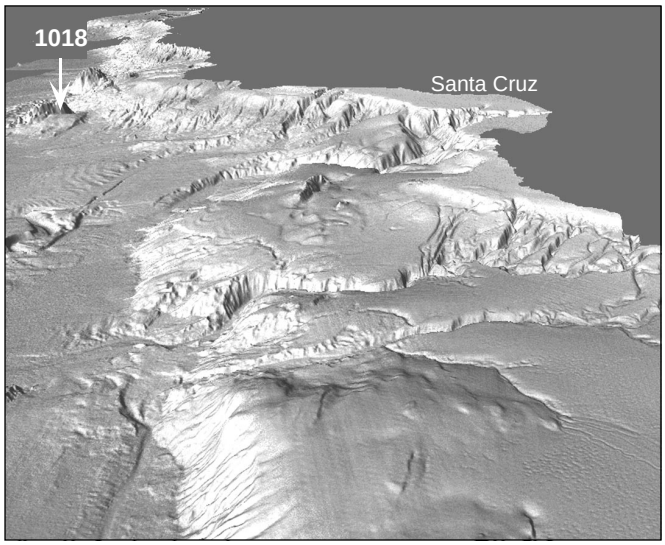

Figure 3. Oblique view of bathymetry along the California Margin toward Site 1018 (from Pratson and Haxby, 1996). The mound of sediments is clearly distinct from Guide Seamount.

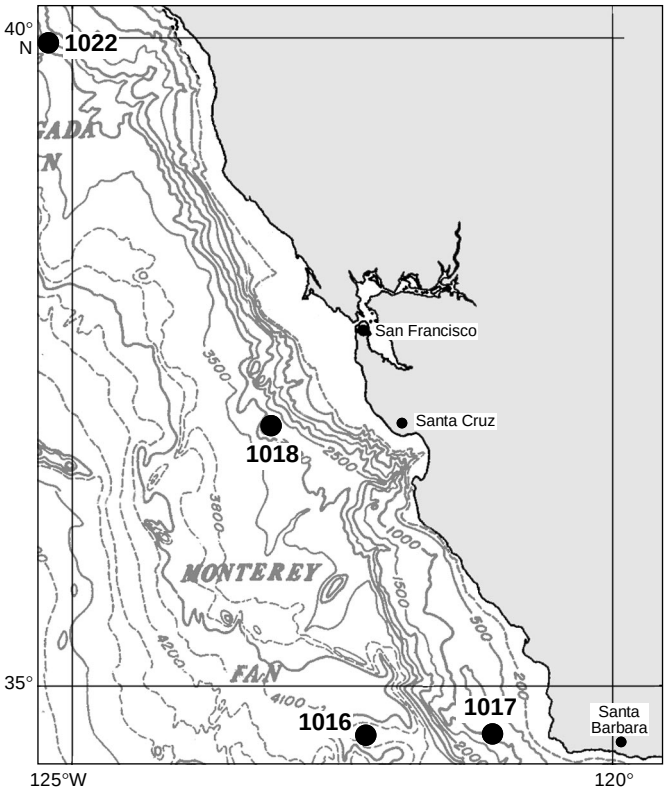

Figure 2. Location map for Site 1018. It is the only Leg 167 site off central California and connects the southern and northern drilling areas.

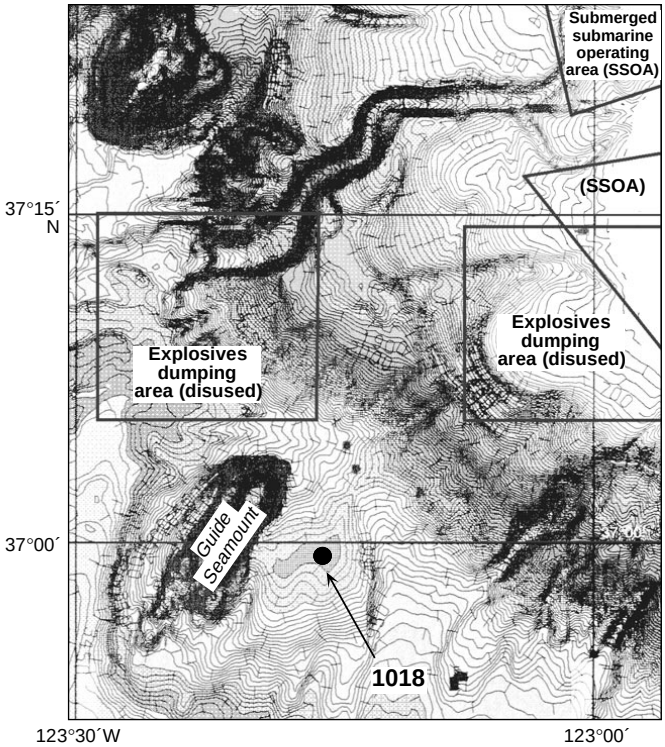

Figure 4. Environmental hazards near Site 1018 on swathmap bathymetry collected by NOAA (Lyle et al., 1995a). Both of the explosives dumping areas are more than 9 km away from the drill site. Site 1018 is located on a sediment mound east of Guide Seamount.

vessel was offset 100 m to the northeast of the Site 1018 coordinates, or 150 m from the object. The results of the camera survey at the new position were negative, and Hole 1018A was spudded at 1830 hr 22 May. APC Cores 167-1018A-1H through 10H were taken down to 90.4 mbsf with 104.4% recovery (Table 1; see Table 2 on CD-ROM in the back pocket of this volume for a more detailed coring summary). Cores 167-1018A-1H and 2H were run through the multisensor track and then were split open to search for artifacts. The search results were negative. Adara temperature measurements were taken on Cores 6H, 8H, and 10H (see "Physical Properties" section, this chapter). XCB Cores 167-1018A-11X through 45X were taken down to 426.2 mbsf with 99.0% recovery. A 30-barrel sepiolite mud pill was circulated, and a wiper trip was performed in preparation for logging. Hole 1018A was logged with density-porosity combination tool string. The logging tool string would not pass below 225 mbsf and was run from 225 to 80 mbsf. The logging tools were rigged down and another wiper trip to bottom was made. The density-porosity tool string was run from 341 to 232 mbsf. The caliper log indicated a large hole diameter, and further logs were canceled.

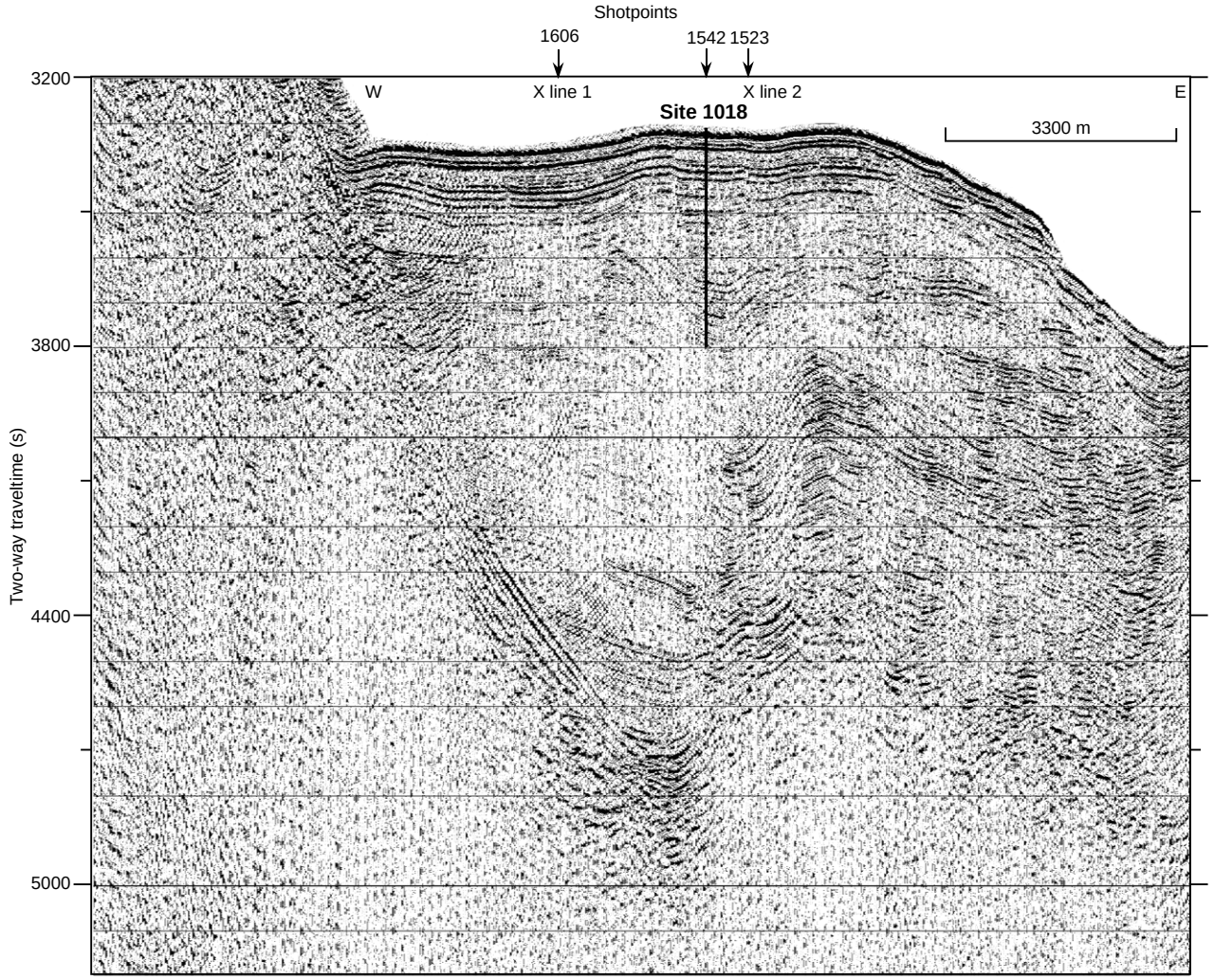

Figure 5. Seismic reflection profile through Site 1018 (Line EW9504 CA8-3; Lyle et al., 1995b). The summed 4-channel data were filtered between 30 and 200 Hz, with predictive deconvolution and Stolt F-K migration applied. The profile cuts across the sediment drift and ends in the west on the slope of Guide Seamount. On y-axis, (s) = milliseconds.

Hole 1018B

Hole 1018B was spudded at 1530 hr on 25 May. APC Cores 167-1018B-1H through 2H were taken from 0 to 19.2 mbsf with 101.3% recovery (Table 1).

Hole 1018C

Hole 1018C was spudded at 1645 hr on 25 May. APC Cores 167-1018C-1H through 10H were taken down to 88.5 mbsf with 104.3% recovery (Table 1). Oriented cores were obtained starting with 167-1018C-3H. XCB Cores 167-1018C-11X through 28X were taken down to 262.2 mbsf with 97.4% recovery.

Hole 1018D

The vessel was offset 10 m to the west, and Hole 1018D was spudded at 1700 hr on 26 May. APC Cores 167-1018D-1H through 11H were taken from 0 to 104.3 mbsf with 101.5% recovery (Table 1). XCB Cores 167-1018D-12X through 18X were taken down to 167.7 mbsf with 96.9% recovery. The drill string was tripped back to the surface and secured for the 48-hr transit to Site 1019 by 1130 hr on 27 May.

LITHOSTRATIGRAPHY

Introduction

A 426-m-thick continuous sequence of upper Pliocene to Quaternary (approximately 0.0–3.4 Ma) sediment was recovered at Site 1018. Sediments vary from siliciclastic to interbedded mixtures of biogenic and siliciclastic components (Fig. 6). Clay is found throughout the cored interval but is predominant in the upper part. The middle part is dominated by diatom clay and diatom clay mixed sediment with frequent interbedding of clayey nannofossil ooze, whereas the lower part is dominated by interbeds of nannofossil clay and clayey nannofossil chalk. Diatomaceous layers tend to be darker and less bioturbated compared with nannofossil-rich layers. Indistinct decimeter-scale bedding superimposed on meter-scale alternation is observed in the upper half of the sequence, whereas meter-scale interbedding predominates in the lower half. Fine-grained feldspar quartz sand occurs as thin, normally graded layers (possibly turbidites), es-

Table 1. Coring summary for Site 1018.

Core	Date (May 1996)	Time	Top (mbsf)	Bottom (mbsf)	Length cored (m)	Length recovered (m)	Recovery (%)
167-1018A-							
1H	23	0150	0.0	4.9	4.9	4.88	99.6
2H	23	0240	4.9	14.4	9.5	9.59	101.0
3H	23	0325	14.4	23.9	9.5	10.03	105.6
4H	23	0420	23.9	33.4	9.5	10.02	105.5
5H	23	0500	33.4	42.9	9.5	10.19	107.2
6H	23	0600	42.9	52.4	9.5	9.95	105.0
7H	23	0640	52.4	61.9	9.5	9.45	99.5
8H	23	0735	61.9	71.4	9.5	9.95	105.0
9H	23	1025	71.4	80.9	9.5	10.07	106.0
10H	23	1125	80.9	90.4	9.5	10.29	108.3
11X	23	1230	90.4	99.1	8.7	8.85	102.0
12X	23	1330	99.1	108.7	9.6	7.14	74.4
13X	23	1445	108.7	118.3	9.6	9.24	96.2
14X	23	1550	118.3	128.0	9.7	9.49	97.8
15X	23	1650	128.0	137.7	9.7	9.68	99.8
16X	23	1800	137.7	147.3	9.6	4.62	48.1
17X	23	1900	147.3	156.9	9.6	9.81	102.0
18X	23	1950	156.9	166.5	9.6	9.95	103.0
19X	23	2030	166.5	176.1	9.6	9.84	102.0
20X	23	2130	176.1	185.7	9.6	9.90	103.0
21X	23	2210	185.7	195.3	9.6	9.82	102.0
22X	24	0000	195.3	204.9	9.6	9.76	101.0
23X	24	0110	204.9	214.5	9.6	9.63	100.0
24X	24	0155	214.5	224.2	9.7	9.82	101.0
25X	24	0240	224.2	233.8	9.6	9.77	102.0
26X	24	0320	233.8	243.5	9.7	9.90	102.0
27X	24	0430	243.5	253.0	9.5	9.83	103.0
28X	24	0510	253.0	262.5	9.5	9.74	102.0
29X	24	0600	262.5	272.2	9.7	9.82	101.0
30X	24	0645	272.2	281.8	9.6	9.76	101.0
31X	24	0745	281.8	291.5	9.7	9.74	100.0
32X	24	0840	291.5	301.1	9.6	9.74	101.0
33X	24	0935	301.1	310.7	9.6	9.78	102.0
34X	24	1050	310.7	320.3	9.6	9.75	101.0
35X	24	1150	320.3	330.0	9.7	9.81	101.0
36X	24	1310	330.0	339.7	9.7	9.78	101.0
37X	24	1420	339.7	349.4	9.7	9.83	101.0
38X	24	1530	349.4	359.0	9.6	9.82	102.0
39X	24	1730	359.0	368.7	9.7	9.84	101.0
40X	24	1915	368.7	378.3	9.6	9.79	102.0
41X	24	2100	378.3	387.9	9.6	9.80	102.0
42X	24	2250	387.9	397.5	9.6	9.55	99.5
43X	25	0035	397.5	407.0	9.5	9.44	99.3
44X	25	0145	407.0	416.7	9.7	9.81	101.0
45X	25	0330	416.7	426.2	9.5	9.58	101.0
167-1018B-							
1H	25	2250	0.0	9.7	9.7	9.68	99.8
2H	25	2330	9.7	19.2	9.5	9.77	103.0
167-1018C-							
1H	26	0000	0.0	6.5	6.5	6.56	101.0
2H	26	0045	6.5	16.0	9.5	9.86	104.0
3H	26	0130	16.0	25.5	9.5	9.88	104.0
4H	26	0210	25.5	35.0	9.5	10.16	106.9
5H	26	0250	35.0	44.5	9.5	10.24	107.8
6H	26	0325	44.5	54.0	9.5	10.01	105.3
7H	26	0410	54.0	63.5	9.5	10.21	107.5
8H	26	0445	63.5	69.5	6.0	6.27	104.0
9H	26	0540	69.5	79.0	9.5	8.93	94.0
10H	26	0620	79.0	88.5	9.5	10.18	107.1
11X	26	0750	88.5	98.2	9.7	7.81	80.5
12X	26	0840	98.2	107.9	9.7	8.95	92.2
13X	26	0930	107.9	117.5	9.6	9.83	102.0
14X	26	1015	117.5	127.2	9.7	9.66	99.6
15X	26	1100	127.2	136.9	9.7	9.69	99.9
16X	26	1145	136.9	146.6	9.7	9.93	102.0
17X	26	1235	146.6	156.3	9.7	9.70	100.0
18X	26	1325	156.3	165.9	9.6	9.86	103.0
19X	26	1420	165.9	175.5	9.6	9.93	103.0
20X	26	1510	175.5	185.2	9.7	9.97	103.0
21X	26	1600	185.2	194.7	9.5	9.90	104.0
22X	26	1650	194.7	204.4	9.7	9.92	102.0
23X	26	1740	204.4	214.0	9.6	9.85	102.0
24X	26	1830	214.0	223.6	9.6	9.89	103.0
25X	26	1915	223.6	233.3	9.7	9.71	100.0
26X	26	2010	233.3	242.9	9.6	4.76	49.6
27X	26	2100	242.9	252.5	9.6	9.94	103.0
28X	26	2150	252.5	262.2	9.7	9.84	101.0
167-1018D-							
1H	27	0010	0.0	9.3	9.3	9.27	99.7
2H	27	0045	9.3	18.8	9.5	9.82	103.0
3H	27	0120	18.8	28.3	9.5	9.53	100.0
4H	27	0155	28.3	37.8	9.5	9.21	96.9
5H	27	0225	37.8	47.3	9.5	9.69	102.0
6H	27	0300	47.3	56.8	9.5	9.19	96.7
7H	27	0330	56.8	66.3	9.5	9.41	99.0

Table 1 (continued).

Core	Date (May 1996)	Time	Top (mbsf)	Bottom (mbsf)	Length cored (m)	Length recovered (m)	Recovery (%)
8H	27	0410	66.3	75.8	9.5	10.25	107.9
9H	27	0440	75.8	85.3	9.5	9.41	99.0
10H	27	0510	85.3	94.8	9.5	10.02	105.5
11H	27	0545	94.8	104.3	9.5	10.12	106.5
12X	27	0640	104.3	110.1	5.8	6.09	105.0
13X	27	0730	110.1	119.7	9.6	8.46	88.1
14X	27	0820	119.7	129.3	9.6	9.80	102.0
15X	27	0910	129.3	138.9	9.6	9.75	101.0
16X	27	1005	138.9	148.5	9.6	9.94	103.0
17X	27	1105	148.5	158.1	9.6	9.58	99.8
18X	27	1200	158.1	167.7	9.6	7.81	81.3

Note: Table 2, on the CD-ROM in the back pocket, this volume, is a more detailed coring summary.

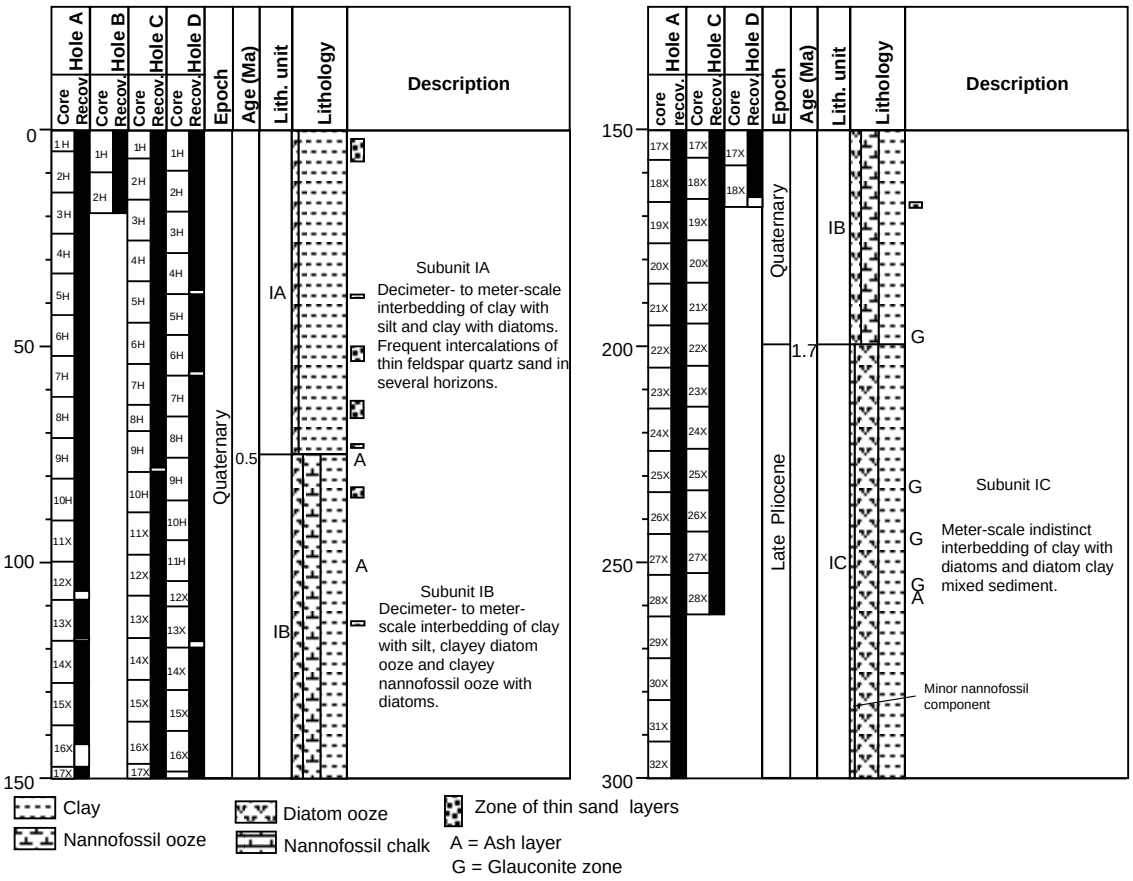

Figure 6. Site 1018 lithostratigraphic summary (0–426.2 mbsf).

pecially in the upper part of the sequence, whereas glauconite occurs both as discrete layers and disseminated in the clay matrix in the lower part of the sequence. Vitric volcanic ash layers are rare except in the lowermost section.

The sediments are divided into two lithostratigraphic units based on visual core descriptions and smear-slide estimates (Fig. 6). Unit I is a siliciclastic unit composed mainly of clays with varying amounts of diatoms and of nannofossils; it is subdivided into three subunits based on variations in the biogenic components. Unit II is characterized by the increased and relatively constant nannofossil content of this calcareous-siliciclastic unit.

Description of Units

Unit I

Hole 1018A, interval 167-1018A-1H-1 through 37X-3; 0–344.2 mbsf;
Hole 1018B, interval 167-1018B-1H and 2H; 0–19.2 mbsf (base of hole);
Hole 1018C, interval 167-1018C-1H-1 through 28X-CC; 0–262.2 mbsf (base of hole);
Hole 1018D, interval 167-1018D-1H through 18X-CC; 0–167.7 mbsf (base of hole).
Age: late Pliocene to Holocene, 0 to 2.8 Ma.

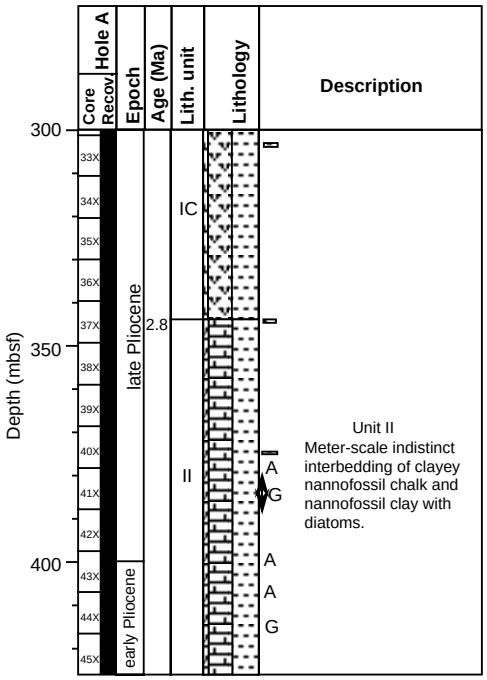

Figure 6 (continued).

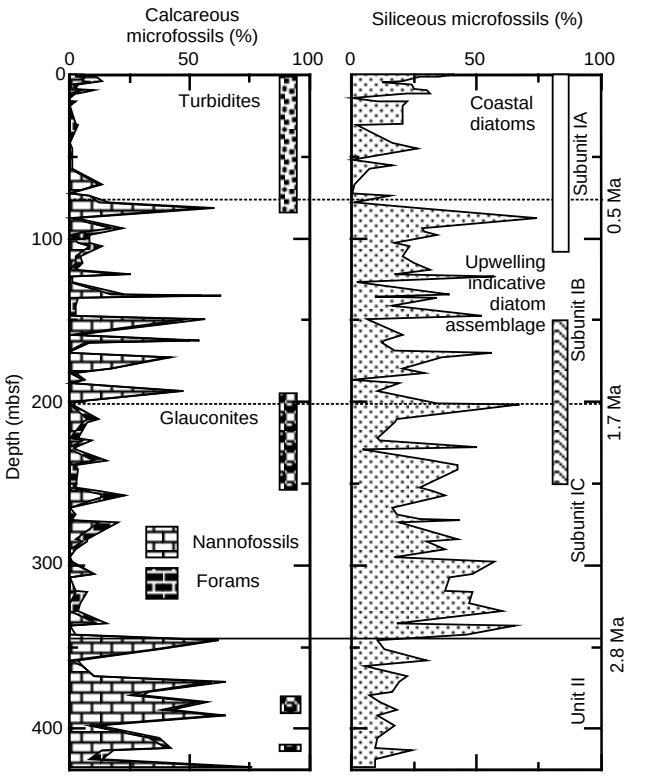

Figure 7. Diagrams showing smear-slide estimates of siliceous and calcareous microfossils content vs. depth.

Unit I is predominantly composed of decimeter- to meter-scale interbeds of darker-colored clay with diatoms and lighter colored clay with or without nannofossils. Thin (<5 cm) feldspar quartz sand layers occur frequently in several intervals of the upper part of this unit, whereas their occurrence is rare in the middle and lower parts. Unit I is subdivided into three subunits based on relative abundance of siliceous and calcareous biogenic components. Contacts between subunits are not strictly defined because of the gradational nature of interbedding in this unit; thus, "intervals" given below are only approximate.

Subunit IA

Hole 1018A, interval 167-1018A-1H-1 through 9H-2; 0–74.4 mbsf;
Hole 1018B, interval 167-1018B-1H and 2H; 0–19.2 mbsf (base of hole);
Hole 1018C, interval 167-1018C-1H-1 through 9H-4; 0–75.5 mbsf;
Hole 1018D, interval 167-1018D-1H through 8H-CC; 0–75.8 mbsf.
Age: Quaternary, 0 to 0.5 Ma.

Subunit IA is characterized by indistinct decimeter-scale beds of olive gray to olive (5Y 4/2 to 5Y 5/3) diatom clay and grayish olive to light grayish olive (10Y 4/1 to 10Y 5/2) clay with silt with gradational boundaries that is superimposed on meter-scale alterations of the same lithologies. The content of siliceous microfossils (mostly diatoms) ranges from 0% to ~30%, whereas the content of calcareous microfossils (nannofossils and foraminifers) ranges from 0% to 15% according to smear-slide estimates (see also "Organic Geochemistry" section, this chapter). Diatom clay layers are darker brown, noncalcareous, and only slightly bioturbated, whereas interbedded lighter grayish-colored layers of clay with silt are moderately bioturbated and occasionally contain small amounts of calcareous microfossils. *Chondrites* burrows are commonly observed near the upper boundaries of the darker layers. Dark gray to grayish olive (N3 to 10Y 4/1) fine-grained feldspar quartz sand with a small amount of green-colored amphibole occurs within several intervals as thin (<5 cm) normally graded layers or small pockets (Fig. 6). Concentrated glauconite grains are found in the basal part of some of these sand layers. Vitric volcanic ash layers are absent in this subunit.

Subunit IB

Hole 1018A, interval 167-1018A-9H-3 through 22X-4; 74.4–201.3 mbsf;
Hole 1018C, interval 167-1018C-9H-5 through 22X-4; 75.5–200.7 mbsf;
Hole 1018D, interval 167-1018D-9H-1 through 18X-CC; 75.8–167.7 mbsf (base of hole).
Age: Quaternary, 0.5 to 1.7 Ma.

The boundary between Subunit IB and Subunit IA is gradational, marked by the appearance of periodic occurrences of nannofossil-rich and/or diatom-rich intervals with increasing depth (Fig. 7). This boundary roughly corresponds to the horizon where the sediment becomes darker (see also color reflectance profile in "Composite Depths and Sedimentation Rates" section, this chapter) and rapid porosity decrease with depth ceases (see "Physical Properties" section, this chapter). The major lithology consists of olive gray (5Y 4/2 to 4/3) clayey diatom ooze, dark gray to grayish olive (5Y 4/1 to 10Y 5/1) clay with diatoms and/or silt, and grayish olive to pale olive (10Y 5/1 to 10Y 6/2) clayey nannofossil ooze that show decimeter- to meter-scale interbedding with gradational contacts. The content of siliceous microfossils (mostly diatoms) ranges from 0% to 75%. The content of calcareous microfossils (mostly nannofossils) ranges from 0% to 65% based on smear-slide estimates (Fig. 7), whereas $CaCO_3$ content ranges from 1% to 16% (see "Organic Geochemistry" section, this chapter). The sediments in this subunit are slightly to moderately bioturbated, and *Chondrites* burrows are commonly visible in darker layers. Thin fine-grained feldspar-quartz sand layers occur in a few horizons but much less frequently than in Subunit IA. Very light gray (N8) fine vitric volcanic ash occurs as a 9-cm-thick layer in Section 167-1018D-11H-4, 47–56 cm. Abundant glauconite grains

disseminated in a clay matrix occur in a 50-cm-thick interval near the base of this subunit.

Subunit IC

Hole 1018A, interval 167-1018A-22X-5 through 37X-3; 201.3–344.2 mbsf;
Hole 1018C, interval 167-1018C-22X-5 through 28X-CC; 200.7–262.2 mbsf (base of hole).
Age: late Pliocene, 1.7 to 2.8 Ma.

The contact of Subunit IC with Subunit IB is gradational and defined by the disappearance of nannofossil-rich intervals and an increase in diatom content with depth (Fig. 7). It also coincides approximately with the disappearance of decimeter-scale high frequency repetition of dark and light layers (see also color reflectance profile in "Composite Depths and Sedimentation Rates" section, this chapter). This subunit consists of meter-scale interbeds of light grayish olive to grayish olive (10Y 5/2 to 10Y 4/1) diatom clay with or without nannofossils and dark gray to dark olive gray (5Y 4/1 to 5Y 3/2) clayey diatom ooze (or diatomite) with indistinct gradational contacts. The content of siliceous microfossils (mostly diatoms) ranges from 5% to 70%, whereas content of calcareous microfossils (nannofossils and foraminifers) ranges from 0% to 20% based on smear slide estimates (Fig. 7; see also "Organic Geochemistry" section, this chapter). A few thin layers of fine-grained feldspar quartz sand with small amounts of glauconite occur in the middle part of this subunit, and 50- to 150-cm-thick intervals with abundant disseminated glauconite in a clay matrix occur in three horizons in the middle and upper parts of this subunit. A 2-cm-thick very light gray (N8) fine vitric volcanic ash layer occurs in Section 167-1018A-28X-4, 3–5 cm. Small, millimeter-scale *Sagarites*(?) deep-water sponges are commonly displayed on the cut surfaces of the cores (Fig. 8).

Unit II

Hole 1018A, interval 167-1018A-37X-4 through 45X-CC; 344.2–426.2 mbsf (base of hole).
Age: early to late Pliocene, 2.8 to 3.5 Ma.

The transition from Unit I to Unit II is gradational and marked by the continuous occurrence and slightly increased content of nannofossils at the expense of diatoms (Fig. 7). These compositional changes also coincide with the interval where bulk and grain densities increase downcore and porosities decrease (see "Physical Properties" section, this chapter). Unit II consists of slightly to moderately bioturbated grayish olive (10Y 4/1) clayey nannofossil chalk and olive gray to dark gray (5Y 4/2 to 5Y 4/1) nannofossil clay with diatoms, which show 3- to 5-m-scale interbedding with gradational contacts. The content of siliceous microfossils (mostly diatoms) ranges from 5% to 30% based on smear-slide estimates (Fig. 7). The content of calcareous nannofossils ranges from 0% to 75% based on smear slide estimates, whereas $CaCO_3$ analysis gives a range of 2% to 25% (see "Organic Geochemistry" section, this chapter). Thin gray (N5) fine vitric and crystal vitric volcanic ash layers occur in the middle part of this subunit. Glauconite occurs as discrete fine-grained sand layers and also disseminated in clay in the middle and lower parts of the subunit.

Depositional History

Sediments at Site 1018 are siliciclastics with small to moderate amounts of siliceous and calcareous biogenic components. Siliciclastics at this site are finer grained than the California Borderland sites (Sites 1012 through 1015) and comparable to offshore Sites 1010 and 1016 based on smear-slide estimates. The overall linear sedimentation rate in this site, however, is above 100 m/m.y., which is 3 to 10 times faster than Sites 1010 and 1016 and equal to or faster than the

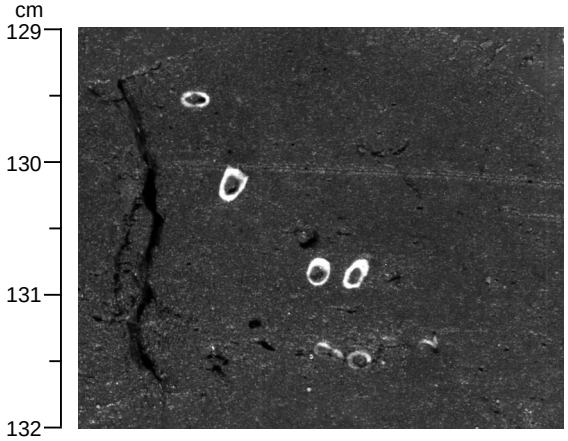

Figure 8. *Sagarites*(?)-type sponges are a common feature of the sediments at Site 1018, as at other sites cored during Leg 167 (Sample 167-1018A-33X-1, 129–132 cm).

Borderland sites (except Site 1015). The fine grain size with high sedimentation rate at this site is consistent with a drift sediment origin (Lyle et al., 1995a). Glauconitic intervals in Subunit IC and Unit II do not correspond to an interval of slower sedimentation during the late Pleistocene and probably did not form in situ. Because the disseminated glauconite grains are medium to coarse grained and occasionally occur in the basal part of sand layers, it is likely that they are derived from downslope transportation. No significant lithostratigraphic changes are observed within the estimated low sedimentation rate interval between 60 and 90 mbsf (see "Biostratigraphy" section, this chapter). The highest sedimentation rate (~200 m/m.y.), estimated for Subunit IA (see "Biostratigraphy" section, this chapter), may be related to increased turbidite deposition, which became frequent after 0.5 Ma (<74 mbsf).

Nannofossils predominate in sediments older than approximately 2.8 Ma (Unit II). This interval corresponds to upper Pliocene nannofossil-rich intervals observed at Sites 1010 through 1014 and 1016. Between 2.8 and 1.7 Ma, diatoms become the dominant biogenic component. This interval is also characterized by a diatom assemblage indicative of high surface productivity conditions (Fig. 7; see also "Biostratigraphy" section, this chapter). Between 1.7 and 0.5 Ma, accumulation of alternating nannofossil-rich and diatom-rich intervals suggests large-scale oscillations in surface water conditions. After 0.5 Ma, abundance of both calcareous and siliceous biogenic components decreased at least partly because of the stronger effect of dilution by siliciclastics, as discussed earlier.

The decimeter-scale interbedding of darker and lighter layers in Subunits IA and IB may be related to millennial-scale oscillations in oxygenation level near the sediment water interface as reflected by changes in the type and intensity of bioturbation between the two (e.g., Savrda et al., 1984). Oscillations in the oxygenation level could be related to changes in type and intensity of surface productivity because darker layers tend to be enriched in diatoms, whereas lighter layers tend to enriched in nannofossils (see also "Biostratigraphy" section, this chapter). These millennial-scale oscillations become more conspicuous in sediments younger than 1.5 Ma (170 mbsf).

BIOSTRATIGRAPHY

The sedimentary sequence recovered from the four holes at Site 1018 consists of a well-dated, apparently continuous 426-m-thick interval of uppermost lower Pliocene to Quaternary sediments. A well-constrained biostratigraphy and chronology for all holes at Site 1018

is provided by a combination of calcareous nannofossil, planktonic foraminifer, radiolarian, and diatom datums for the upper Pliocene and Quaternary. Planktonic foraminifers suggest that the base of the section is about 3.4 Ma in age. An age/depth plot for Hole 1018A (Fig. 9) suggests two changes in sedimentation rate during the late Quaternary (last 800 k.y.) preceded by a remarkably long, continuous rate of sedimentation from the early Quaternary to the latest early Pliocene. The sequence contains common to abundant radiolarians and diatoms throughout. Radiolarians are well preserved and diatoms moderately well preserved. Calcareous nannofossils exhibit highly variable abundances and quality of preservation in the Quaternary and the upper upper Pliocene, and are generally common to abundant and of moderate preservation in the lower upper Pliocene. Planktonic foraminifers are common to abundant and well preserved in the middle and upper Quaternary, but are much less abundant and well preserved in lower levels of the sequence. Benthic foraminifers are essentially continuous throughout and are especially well preserved in the Quaternary and uppermost Pliocene.

All of the microfossil groups at Site 1018 are clearly dominated by cool, high-latitude elements throughout the late Neogene. Site 1018 is sufficiently far north in the California Current to exclude most to all subtropical elements even during interglacial episodes. Radiolarians are entirely represented by subarctic forms. Diatoms are dominated by subarctic forms, with the addition of much less abundant temperate elements. Discoasters are absent to rare above the middle upper Pliocene (younger than 2.6 Ma). Planktonic foraminifer assemblages are dominated by subarctic to cool temperate forms, with subtropical elements absent except during warmest interglacial episodes. Planktonic foraminifers exhibit glacial to interglacial oscillations throughout. Radiolarians, however, do not exhibit such changes, almost certainly because they largely live at greater water depths.

Changes in microfossil assemblages provide evidence of progressive cooling during the late Neogene. The first consistent occurrence of mostly common to abundant populations of sinistrally coiled *Neogloboquadrina pachyderma* marks a distinct cooling step at ~1.3 Ma. Likewise, changes in radiolarian assemblages indicate a further step towards cooler conditions at about 1.0 Ma. Diatoms are dominated by oceanic forms, but, during the Quaternary, include a small but distinct littoral assemblage that typically lives on sea grass. These forms were reworked from shallow waters and appear to be most abundant during times of higher input of terrigenous sediments.

Middle and upper Quaternary benthic foraminifer assemblages exhibit clear oscillations associated with glacial-interglacial episodes as inferred from changes in planktonic foraminifers.

Planktonic Foraminifers

Site 1018 contains a moderately good and apparently continuous sequence of planktonic and benthic foraminifers of latest early Pliocene (~3.4 Ma) through Holocene age (Table 3). The base of Hole 1018A (Sample 167-1018A-45X-CC) is in the uppermost Pliocene, immediately below the lower/upper Pliocene boundary based on the FO of *Globorotalia inflata* in Sample 167-1018A-43X-CC.

Planktonic foraminifers exhibit highly variable abundances throughout (Table 3). They are generally common to abundant and well preserved through much of the Quaternary above 186 mbsf (Sample 167-1018A-20X-CC). Below this level, planktonic foraminifers are few and exhibit moderate to poor preservation. Within this interval there are also a number of barren intervals. Benthic foraminifers occur in almost all core-catcher samples in variable abundances. They are generally abundant and well preserved throughout most of the Quaternary and uppermost Pliocene and are generally less abundant and well preserved throughout the upper Pliocene below 243 mbsf (Sample 167-1018A-26X-CC).

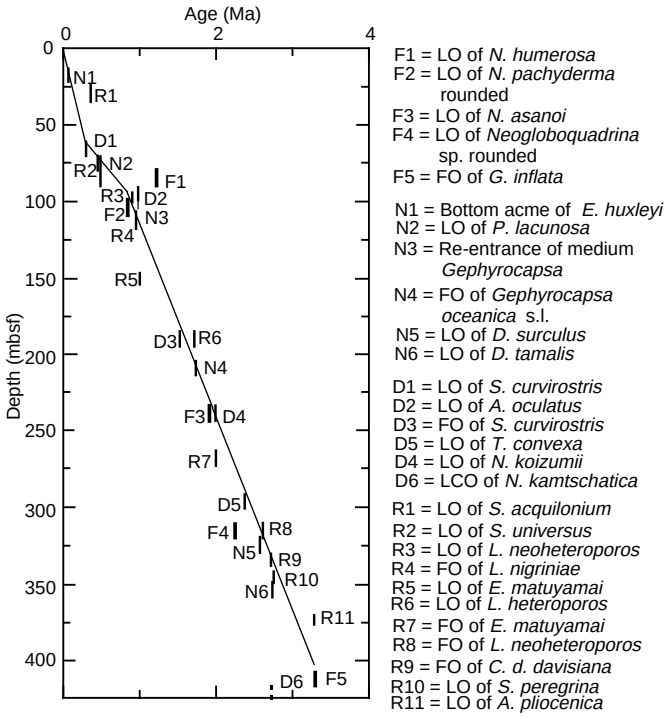

Figure 9. Age/depth plot for Hole 1018A.

The planktonic foraminifer sequence at Site 1018 is similar to that found in upper Pliocene and Quaternary sequences cored at Sites 1010 through 1016. In Hole 1018A we arbitrarily place the base of the Quaternary at 205 mbsf (between Samples 167-1018A-23X-CC and 22X-CC) at the level of the FO of *Neogloboquadrina pachyderma* sp. (rounded form), which is observed between the LO of *Neogloboquadrina asanoi* and before the LO of *Neogloboquadrina humerosa.* In Hole 1018C, this level was observed at 185 mbsf (between Samples 167-1018C-21X-CC and 20X-CC). We recognized a sequence of four useful datum levels in the Quaternary through upper Pliocene as follows: LO of *N. pachyderma* sp. (rounded form) at 0.9 Ma (Samples 167-1018A-12X-CC, 167-1018C-14X-CC, and 167-1018D-12X-CC); LO of *N. asanoi* at 1.9 Ma (Samples 167-1018A-27X-CC and 167-1018C-27X-CC); LO of *Neogloboquadrina* sp. (rounded) at 2.25 Ma (Sample 167-1018A-34X-CC); and FO of *G. inflata* at 3.3 Ma (Sample 167-1018A-43X-CC). Also, the LO of *N. humerosa* in Hole 1018A was observed in Sample 167-1018A-11X-CC at 99 mbsf, although in Hole 1018C the last occurrence of this species was observed in Sample 167-1018C-7H-CC at 63 mbsf. The first consistent occurrence of mostly common to abundant populations of sinistral *N. pachyderma* occurs in the lower Quaternary in Samples 167-1018A-17X-CC and 167-1018C-15X-CC (Tables 3, 4).

Planktonic foraminifer assemblages at Site 1018 are made up entirely of cool-temperate to subarctic taxa. Warm-subtropical forms such as *Globigerinoides ruber* are no longer observed even in interglacial assemblages, because of the cooler, higher latitude location of Site 1018. The assemblages are distinctly cool throughout and the diversity within the faunas is generally low. Nevertheless, the assemblages clearly reflect glacial to interglacial oscillations throughout. These are especially conspicuous during the middle and upper Quaternary above 157 mbsf (Sample 167-1018A-27X-CC).

Benthic foraminifers in the sequence are typical middle bathyal deep-sea assemblages. Faunas above 128 mbsf (Sample 167-1018A-14X-CC) typically contain species of *Uvigerina, Cibicidoides, Bulimina, Globobulimina, Oridorsalis, Hoeglundina, Gyroidina,*

Table 3. Distribution and relative abundances of planktonic foraminifers in Hole 1018A.

Zone	Core, section, interval	Depth (mbsf)	Abundance	Preservation	*Globorotalia inflata*	*Globorotalia punticulata*	*Globorotalia scitula*	*Globorotalia hirsuta*	*Globorotalia truncatulinoides*	*Neogloboquadrina dutertrei*	*Neogloboquadrina humerosa*	*Neogloboquadrina asanoi*	*Neogloboquadrina* sp. "rounded"	*Neogloboquadrina pachyderma* "rounded"	*Neogloboquadrina pachyderma* dex.	*Neogloboquadrina pachyderma* sin.	*Globigerina bulloides*	*Globigerina umbilicata*	*Globigerina apertura*	*Globigerina quinqueloba*	*Globigerinita glutinata*	*Hastigerina aequilateralis*	*Orbulina universa*	*Globorotaloides hexagona*
	167-1018A-																							
	1H-CC	5	A	G			R									A	A				R			
	2H-CC	14	A	G			R									A	A							
	3H-CC	24	A	G			R									A	A	A			F			
	4H-CC	33	C	G												A	A							
	5H-CC	43	F	G												F								
	6H-CC	52	F	M											R	C	C			R				
	7H-CC	62	A	G			R		R	A					A	F	A					C	C	
	8H-CC	71	A	G												A	A	A						
	9H-CC	80	A	G	C		R								F	A	A						F	
	10H-CC	90	C	G	C											A	A							
N22/23	11X-CC	99	A	G			R			C	C				A	C	A	F			R		R	
	12X-CC	109	C	G			R				F			F	C	C								R
	13X-CC	118	R	P												R	R							
	14X-CC	128	A	G	R		R	R								A	A							
	15X-CC	138	F	M											C	F								
	16X-CC	148	A	G										A		A	A		C					
	17X-CC	157	A	G	R			R						A		A	A			A				
	18X-CC	167	B																					
	19X-CC	176	F	M										F	F	F	C							
	20X-CC	186	A	G										C	A		A							
	21X-CC	195	R	P										R			C	R	R					
	22X-CC	205	F	M										C	F		A	A		F				
	23X-CC	215	B																					
	24X-CC	224	R	P													R							
	25X-CC	234	F	M							F				C	R	A							
	26X-CC	244	F	M											C		A							
	27X-CC	253	F	M								C					C							
	28X-CC	263	R	P								R					R							
	29X-CC	272	F	M								F			R	R	A						R	
	30X-CC	281	R	P								R					R							
	31X-CC	292	F	M								F			R		F							
	32X-CC	301	B																					
N21	33X-CC	311	B																					
	34X-CC	320	C	M	F		R					C	C		C		A							
	35X-CC	330	F	M								C	C				C						R	
	36X-CC	340	R	P								F					F						R	
	37X-CC	349	F	M	R							F					F							
	38X-CC	359	B																					
	39X-CC	369	F	M								C	F		C		C							
	40X-CC	378	R	P								F					F				R			
	41X-CC	388	B																					
	42X-CC	397	R	P								R												
	43X-CC	407	F	M	C							C			R		C						R	
N20	44X-CC	417	F	M																			R	
	45X-CC	426	F	M		R		R			R						C			F			C	

Note: See "Explanatory Notes" chapter for abbreviations.

Chilostomella, Melonis, Pyrgo, and *Pullenia.* Below this level, faunas differ in containing distinctly higher abundances of nodosariids, *Plectofrondicularia, Stilostomella,* and generally have lower frequencies of *Uvigerina.* Middle and upper Quaternary benthic foraminifers assemblages exhibit clear oscillations associated with glacial-interglacial episodes as inferred from changes in planktonic foraminifers. Interglacial assemblages are marked by the presence of relatively common *Uvigerina peregrina dirupta, U. proboscidea, U. hispida,* and *Cibicidoides wuellerstorfi.* Glacial assemblages, in contrast, are marked by abundant *U. senticosta,* relatively low abundances of other species of *Uvigerina,* and high abundances of *Bulimina striata mexicana.* The conspicuous changes in benthic foraminifer assemblages at Site 1018, between glacial and interglacial episodes during the middle and late Quaternary, reflect either changes in thermohaline circulation at these middle bathyal water depths (2500 m) or changes in surface-water productivity that affected oxygen levels on the seafloor and/or the food supply of benthic foraminifers between glacial and interglacial episodes.

Calcareous Nannofossils

Calcareous nannofossils are absent to common and poorly to well preserved through the Quaternary and upper upper Pliocene in Holes 1018A and 1018C. In the middle upper Pliocene, calcareous nannofossils are generally common to abundant and preservation is moderate (Table 5). Discoasters in the upper upper Pliocene are rare or absent, because of cooling conditions at this higher latitude location. Below this interval (~2.6 Ma), they are few or common. Hole 1018A spans late Pliocene Zone CN12a to late Pleistocene Zone CN15, and Hole 1018C is dated from latest Pliocene Zone CN12d to late Pleis-

Table 4. Coiling dominance of *Neogloboquadrina pachyderma* in Hole 1018C.

Core, section, interval	Depth (mbsf)	*Neogloboquadrina pachyderma* coiling dominance
167-1018C-		
1H-CC	7	Sinistral
2H-CC	16	Sinistral
3H-CC	26	Sinistral
4H-CC	35	Sinistral
5H-CC	44	Sinistral
6H-CC	54	Sinistral/Dextral
7H-CC	63	Sinistral/Dextral
8H-CC	69	—
9X-CC	79	Sinistral
10X-CC	88	Sinistral
11X-CC	98	Sinistral
12X-CC	107	Sinistral
13X-CC	117	—
14X-CC	128	Sinistral
15X-CC	137	Sinistral/Dextral
16X-CC	147	—
17X-CC	156	—
18X-CC	166	—
19X-CC	176	Dextral
20X-CC	185	Dextral
21X-CC	195	Dextral
22X-CC	204	Dextral
23X-CC	214	—
24X-CC	224	Dextral
25X-CC	233	Sinistral/Dextral
26X-CC	243	Dextral
27X-CC	253	Dextral
28X-CC	262	Dextral

Note: — = insufficient data to analyze.

tocene Zone CN15. Datums recognized within the Quaternary are the bottom of acme of *E. huxleyi,* the LO of *P. lacunosa,* and the FO of *Gephyrocapsa oceanica* s.l. In the Quaternary, calcareous nannofossil assemblages are marked by the presence of *Emiliania huxleyi, Pseudoemiliania lacunosa, Calcidiscus leptoporus, Helicosphaera carteri, H. sellii,* and several morphotypes of *Gephyrocapsa* spp.

The FO of *G. oceanica* s.l. places the Pliocene/Pleistocene boundary at 204.90 mbsf (Sample 167-1018A-22X-CC) at Hole 1018A and at 204.40 mbsf (Sample 167-1018C-22X-CC) at Hole 1018C. Pliocene nannofossil assemblages are marked by an association of *Helicosphaera carteri, H. sellii, Discoaster brouweri, D. tamalis, D. pentaradiatus, D. surculus, Ceratolithus* spp., and several morphotypes of *Reticulofenestra.*

Diatoms

Diatoms are generally common to abundant and poorly to moderately well preserved throughout the Quaternary through upper Pliocene section recovered at Site 1018. In the uppermost parts of the Quaternary section, however, diatoms are few because of increases in clay minerals and silt grains.

Diatom assemblages from all core-catcher samples consist almost entirely of oceanic species, occasionally including littoral benthic forms. They are mainly of the subarctic North Pacific Ocean, although such warm-water taxa as *Hemidiscus cuneiformis, Nitzschia reinholdii, Pseudoeunotia doliolus, Azpeitia nodulifer,* and *Thalassiosira convexa* are typically present throughout the section.

The core-catcher samples examined range from the Quaternary *Neodenticula seminae* Zone (NPD 12) to the late Pliocene *Neodenticula koizumii-Neodenticula kamtschatica* Zone (NPD 8). The Neogene North Pacific Ocean diatom zones are readily distinguishable, and standard diatom datum levels were used to recognize these zones. Minor displacement of diatom zonal boundaries, however, is apparent between Holes 1018A and 1018C (Tables 6, 7).

The boundary between the late Quaternary *N. seminae* and *Simonseniella curvirostris* Zones (NPD 12/11) is clearly indicated by the LO of *S. curvirostris* around 70 mbsf among the three Holes 1018A, 1018C, and 1018D (Table 8). The continuous occurrence of *P. doliolus* is observed from the NPD 11 through the upper part of Zone NPD 10 (Samples 167-1018A-8H-CC through 14X-CC). This species is one of the most diagnostic forms within the low-latitude diatom zonation (Baldauf and Iwai, 1995), and its stratigraphic distribution probably indicates the proximity of warm surface waters (Table 6).

The LO of *Actinocyclus oculatus* in Sample 167-1018A-11X-CC marks the boundary between the *S. curvirostris* and *A. oculatus* Zones (NPD 11/10) in Hole 1018A, but it is not detected in Holes 1018C and 1018D. Within Zone NPD 10, the FO of *S. curvirostris* between Samples 167-1018A-20X-CC and 21X-CC may be useful for subdividing this zone. This datum, with an assigned age of 1.58 Ma, is tentatively adapted as a zonal boundary between Zones NPD 11 and 10 (between Samples 167-1018C-20X-CC and 21X-CC) in Hole 1018C, because the LO of *A. oculatus* was not observed. The short range of *Rhizosolenia matuyamai,* which ranges from only 1.04 to 1.2 Ma, supports this biostratigraphic determination.

Koizumi (1992) proposed that the base of the *A. oculatus* Zone (NPD 10) and top of the underlying *N. koizumii* Zone (NPD 9) is defined by the LO of *N. koizumii.* This latest Pliocene event at 2.0 Ma occurs between Cores 25X-CC and 26X-CC in both Holes 1018A and 1018C. The LO of *T. convexa* (2.4 Ma) is documented in the middle of Zone NPD 9 between Samples 167-1018A-31X-CC and 32X-CC.

The LCO (last common occurrence) of *N. kamtschatica* between Samples 167-1018A-44X-CC and 45X-CC marks the top of the underlying *N. koizumii-N. kamtschatica* Zone (NPD 8). According to Koizumi and Tanimura (1985), Koizumi (1992), and Barron and Gladenkov (1995), the FO of *N. seminae* should fall immediately below this datum level. However, the lowest record of *N. seminae* in Samples 167-1018A-40X-CC does not support this placement within the top of Zone NPD 8 in Hole 1018A. This discrepancy indicates that the LCO of *N. kamtschatica* is diachronous and appears to be earlier than in the subarctic region.

In contrast to the late Pliocene to Quaternary diatom assemblages at 1016, those of Site 1018 contain consistent, but typically few, neritic diatoms. These taxa include representatives of the littoral benthic genera *Cocconeis, Gomphonema,* and *Diploneis,* and are taken as evidence for sediment transported from the west coast continental shelf or the top of Guide Seamount, if this was within the photic zone. The transport of these diatoms must have been contemporaneous, because reworked diatoms are extremely rare in Site 1018 sediments.

During the uppermost Pliocene to lower Pleistocene, the diatom assemblages are marked by common *N. seminae,* rare-to-few *Rhizosolenia barboi,* and *Stephanopyxis turris,* which are indicative of high oceanic-to-marginal productivity. The abundant fragments of *Thalassiothrix* species and large numbers of siliceous bands dislodged from diatom girdles, found sometimes in this interval, may be an indication of surface-water oscillations associated with climatic change.

Radiolarians

Radiolarians are few to abundant and well preserved in Holes 1018A, 1018B, and 1018C.

All core catchers were processed. Relative abundances of 42 stratigraphically significant species were estimated at Hole 1018A (Table 9). Stratigraphic events were only recognized in samples from Holes 1018C and 1018D (Table 10).

The consistent occurrence of *Eucyrtidium matuyamai* and the LO of *Lamprocyrtis heteroporos* place the Pliocene/Pleistocene boundary between 185.7 and 195.3 mbsf in Hole 1018A, 175.5 and 185.2 mbsf in Hole 1018C, respectively. The base of Hole 1018D is slightly younger than the boundary. The location of the upper limit of the *Stylatractus universus* Zone (the LO of *S. universus* at 0.42 to 0.5 Ma) is well recognized only at Hole 1018C. Relatively poor radiolarian assemblages in samples from Holes 1018C and 1018D do not permit placement of this zonal boundary. Radiolarian events are generally

Table 5. Distribution and relative abundances of calcareous nannofossils in Holes 1018A, 1018B, and 1018C.

Zone	Core, section, interval (cm)	Depth (mbsf)	Preservation	Abundance	*Emiliania huxleyi*	*Pseudoemiliania lacunosa*	*Helicosphaera carteri*	*Helicosphaera sellii*	*Gephyrocapsa oceanica* s.l.	*Gephyrocapsa* sp. 3	*Gephyrocapsa* small	*Discoaster brouweri*	*Discoaster pentaradiatus*	*Discoaster surculus*	*Discoaster tamalis*	*Ceratholithus* spp.	*Coccolithus pelagicus*	*Calcidiscus macintyrei* >11 µm	*Calcidiscus leptoporus*
	167-1018A-																		
CN15	1H-CC	4.90	G	C	P				F		C						F		R
CN15	2H-CC	14.40	G	F/C	P				C		P						R		
CN15–CN14b	3H-CC	23.90	P	R/F			R	cf	P		P						R		
CN15–CN14b	4H-CC	33.40	G	C					P		C						F		R
	5H-CC	42.90		B															
	6H-CC	52.40	P	RR													RR		
CN15–CN14b	7H-CC	61.90	G	C/A			C		C		A						F/C		R
	8H-CC	71.40	P	RR							P								
CN14a?	9H-CC	80.90	G	C		RR	F		C		A						R		
CN14a	10H-CC	90.40	G	R		F			P		P								
CN14a	11X-CC	99.10	M	R/F		C			R		C								R
CN14a–CN13b	12X-CC	108.70	P	C							C						C		
	13X-CC	118.30		B															
CN14a–CN13b	14X-CC	128.00	P	R		P											R		R
	15X-CC	137.70	P	RR		R													
CN14a–CN13b	16X-CC	147.30	P	R		P					P						R		R
CN14a–CN13b	17X-CC	156.90	M/G	A		C					C						F		F
	18X-CC	166.50		B															
	19X-CC	176.10		B															
CN13b	20X-CC	185.70	M	C/A		C		C	P		A						C		R
CN13b	21X-CC	195.30	P	R		R			R										
CN13b	22X-CC	204.90	P	R		R		R	R										
CN12–CN13a	23X-3, 20	208.10	P	R/F		C													F
	23X-5, 20	211.10		B															
	23X-CC	214.50		B															
	24X-3, 20	217.70		B															
	24X-5, 20	220.70		B															
	24X-CC	224.20	P	R		R											R		
CN12–CN13a	25X-CC	233.80	M	F		R	R	F/R										RR	
CN12–CN13a	26X-CC	243.50	M	C		F		R										RR	F
CN12–CN13a	27X-CC	253.00	P	F		P		C										R	F
CN12–CN13a	28X-CC	262.50	P	R/F		P	R										F	R	
	29X-CC	272.20	P	RR		P													
	30X-CC	281.80	P	RR													R	R	
	31X-CC	291.50		B															
	32X-CC	301.10		B															
	33X-CC	310.70		B															
CN12c	34X-CC	320.30	M/G	A		C							RR				C		R
CN12b	35X-CC	330.00	M	C		C								R				C	R
CN12b	36X-CC	339.70	P	R								R		P					
	37X-CC	349.40	P	RR		R													
CN12a	38X-CC	359.00	M	C/A		C								F	R/F		F		F
CN12a	39X-CC	368.70	G	A								R	R/F		R		F	C	
CN12a	40X-CC	378.30	M/G	A		C							R	F			F	R	
CN12a	41X-CC	387.90	G	C		P								R			F		F
CN12a	42X-CC	397.50	G	A		P	R	R					F	F	F/R	R		C	
CN12a	43X-CC	407.00	G	A		R		R					F	F	F		C	C/F	
CN12a	44X-CC	416.70	M/P	C		P							R	P	R			C	
CN12a	45X-CC	426.20	G	A		P											F	R	R
	167-1018B-																		
CN15	1H-CC	9.70	M	C	P		R		F		C						R		
CN15	2H-CC	19.20	M	F	P				F		C						R		
	167-1018C-																		
CN15	1H-CC	6.50	M	F/C	P				F		C						F		
CN15	2H-CC	16.00	M	F	P						C						F		
CN15	3H-CC	25.50	M/G	C	P		R		R		C						F		
CN15–CN14b	4H-CC	35.00	M	F/C	?		R		R		C						F/C		R
	5H-CC	44.50		B															
	6H-CC	54.00		B															
CN15–CN14b	7H-CC	63.50	M/G	C					C		A						F		
CN15–CN14b	8H-CC	69.50	P	R/F					R		C						R		
CN15–CN14b	9H-CC	79.00	P	F					R	RR	P								RR
CN14a	10H-CC	88.50	P	R/F		R			R								C		R
CN14a	11X-CC	98.20	M/G	C		F			RR		D						F		
CN14a	12X-CC	107.90	M/G	C/A		C	R		P		D								R
	13X-CC	117.50		B															
	14X-CC	127.20		B															
CN13b?	15X-CC	136.90	M	A		C					P								R
	16X-CC	146.60		B															
	17X-CC	156.30		B															
	18X-CC	165.90	P	RR		P													
	19X-CC	175.50		B															
CN13b	20X-CC	185.20	P	R		R			P										P
	21X-CC	194.70		B															
CN13b	22X-CC	204.40	P	R		P			P										R
	23X-CC	214.00	P	RR		R													R

Table 5 (continued).

Zone	Core, section, interval (cm)	Depth (mbsf)	Preservation	Abundance	*Emiliania huxleyi*	*Pseudoemiliania lacunosa*	*Helicosphaera carteri*	*Helicosphaera sellii*	*Gephyrocapsa oceanica* s.l.	*Gephyrocapsa* sp. 3	*Gephyrocapsa* small	*Discoaster brouweri*	*Discoaster pentaradiatus*	*Discoaster surculus*	*Discoaster tamalis*	*Ceratholithus* spp.	*Coccolithus pelagicus*	*Calcidiscus macintyrei* >11 µm	*Calcidiscus leptoporus*
CN13a	24X-CC	223.60	P/M	F		R	R	R/F											C
CN13a	25X-CC	233.30	M	C/A				F									F	R	F/R
	26X-CC	242.90		B															
CN12d?	27X-CC	252.50	M/G	C		R/F		F				RR					F	C	R
CN12d	28X-CC	262.20	G	A		C						R					C		C

Note: See "Explanatory Notes" chapter for abbreviations.

well correlated at the three holes. The LO of *Lamprocyrtis neoheteroporos* was, however, recognized at a relatively high level in Hole 1018D, which is roughly 20 m above the location of the same datum levels in Holes 1018A and 1018C.

Abundant and well-preserved assemblages contain species that are indicative of subarctic conditions throughout all the sequence. Relatively high abundances of *Amphimelissa setosa*, *Pterocorys korotnevi*, *Stylotrochus glacialis*, and large discoidae suggest cooler arctic conditions above the LO of *E. matuyamai* at 1 Ma. Occurrence of species endemic to upwelling areas are scarce throughout the sequence, suggesting weaker upwelling conditions at this site compared with Site 1016 during the entire upper Pliocene to Quaternary.

PALEOMAGNETISM

At Hole 1018A, the archive halves of 10 APC cores and sections of the subsequent 15 XCB cores were magnetically measured with the pass-through cryogenic magnetometer. After measuring the natural remanent magnetization (NRM), the sections were demagnetized with a peak alternating field (AF) of 20 mT. The working halves of Cores 167-1018C-1H to 10H and 167-1018D-10H and 11H were only measured after AF demagnetization at 20 mT. The NRM intensity ranged mainly between 5 and 20 mA/m down to 230 mbsf, except for the top 7 mbsf of each hole, where the NRM intensity increased to about 300 mA/m (Figs. 10, 11). After AF cleaning, the intensity was reduced to values between 0.3 and 3 mA/m in the APC cores in the top 90 mbsf. After AF treatment, the magnetization of most XCB sections was below the sensitivity limit of the magnetometer (<0.7 mA/m). Quite likely the positive inclinations of the APC cored sections (top 88 mbsf) of Holes 1018A and 1018C represent the Chron C1n (Brunhes). The two deepest APC cores in Hole 1018D (10H and 11H) had normal polarity after AF demagnetization and extend the Brunhes magnetozone at least down to 104 mbsf.

The best preserved sections of each XCB core from Hole 1018A were measured with the cryogenic magnetometer before and after AF demagnetization at 20 mT with the aim of detecting the Brunhes/Matuyama transition. Demagnetization of these XCB cores (Fig. 10) did not reveal an interval with negative inclinations (reverse polarity). Below the APC cored interval of normal polarity (0–104 mbsf) an interpretation of the inclination record was not possible because of the low magnetic intensity and drilling disturbance of most cores.

Ten discrete samples from Cores 167-1018A-11X to 15X were stepwise AF demagnetized and measured with the Minispin magnetometer, because the Brunhes/Matuyama chronozone boundary was expected in this interval based on biostratigraphic datums (see "Biostratigraphy" section, this chapter). After removal of a steeply normal drilling-induced overprint, all samples have positive inclinations (Table 11). One possible explanation for the lack of a reversed polarity interval could be the insufficient removal of a normal overprint or the insufficient sensitivity of the spinner magnetometer. The sensitivity limit is at approximately 0.1–0.2 mA/m using the long spinning option and 6 orientations of the sample.

COMPOSITE DEPTHS AND SEDIMENTATION RATES

Multisensor track (MST) data collected at 4-cm intervals from Holes 1018A through 1018D, and color reflectance data collected at 6- to 10-cm intervals from Holes 1018A, 1018C, and 1018D were used to determine depth offsets in the composite section. On the composite depth scale (expressed as mcd, meters composite depth), features of the plotted MST and color reflectance data present in adjacent holes are aligned so that they occur at approximately the same depth. Working from the top of the sedimentary sequence, a constant was added to the mbsf (meters below sea floor) depth for each core in each hole to arrive at a mcd depth for that core. The depths offsets that compose the composite depth section are given in Table 12 (also on CD-ROM, back pocket). The continuity of the sedimentary sequence was documented for the upper 193 mcd.

Color reflectance was the primary parameter used for interhole correlation purposes. Magnetic susceptibility and GRAPE density measurements were used in many instances to provide additional support for composite construction. Natural gamma-ray activity measurements were made throughout the entire section in Holes 1018A, 1018B, and 1018C, but the sampling interval of 12 cm was insufficient for interhole correlation.

The color reflectance, magnetic susceptibility, and GRAPE records used to verify core overlap for Site 1018 are shown on a composite depth scale in Figures 12, 13, and 14, respectively. The GRAPE data were used to identify intervals of voids and highly disturbed sediments (values <1.45 g/cm^3), and all MST and color reflectance data were culled from these intervals. The cores from Holes 1018A, 1018C, and 1018D provide nearly continuous overlap to about 193 mcd. Cores from Holes 1018A and 1018C were placed into composite depth over the interval from 193 to 283 mcd, but core gaps could not be covered in many cases (e.g., see core gaps at 203, 213, and 245 mcd in Fig. 12). The composite records suggest that up to 5 m of material may be missing between cores down to about 193 mcd, although the average gap is l to 2 m. As there are no data to fill possible core gaps below 193 mcd, an assessment of core gap length below this depth is not possible.

Following construction of the composite depth section for Site 1018, a single spliced record was assembled from the aligned cores using color reflectance data where available and GRAPE data in intervals where reflectance data were not collected. Cores from Hole 1018C were used as the backbone of the sampling splice. Cores from Holes 1018D primarily were used to splice across core gaps in Hole 1018C with cores from Hole 1018A used in several places. The com-

Table 6. Distribution and relative abundances of diatoms in Hole 1018A.

Geologic age	North Pacific diatom zone	Numeric age (Ma)	Core, section, interval	Sample depth (mbsf)	Group abundance	Preservation	Environment	*Actinocyclus curvatulus*	*Actinocyclus ehrenbergii*	*Actinocyclus ingens*	*Actinocyclus oculatus*	*Actinoptychus senarius*	*Amphora* sp.	*Aulacosira granulata*	*Azpeitia nodulifer*	*Biddulphia aurita*	*Coconeis californica*	*Cocconeis* cf. *californica*	*Cocconeis costata*	*Cocconeis decipiens*	*Cocconeis scutellum*	*Cocconeis* sp.	*Coscinodiscus marginatus*	*Coscinodiscus radiatus*	*Coscinodiscus* sp.	*Cymbella* sp.	*Delphineis* spp.	*Denticulopsis hustedtii*	*Denticulopsis hyalina*	*Denticulopsis lauta*	*Denticulopsis lauta* s.l.	*Epithemia* sp.	*Gomphonema* sp.	*Grammatophora* sp.	*Hemidiscus cuneiformis*	*Navicula* sp.	*Neodenticula kamtschatica*	*Neodenticula* cf. *kamtschatica*
			167-1018A-																																		
		0.00	1H-CC	4.9	F	P	Coastal					C													F									R		
			2H-CC	14.4	C	P/M						R	R	R								R										T				
			3H-CC	23.9	F	P												R																		
	NPD 12		4H-CC	33.4	C	M	Coastal	R				R																						R		
			5H-CC	42.9	F	M																												T		
			6H-CC	52.4	R	P/M								T													T									
		0.30	7H-CC	61.9	C	P/M	Coastal															T										T				
	NPD 11		8H-CC	71.4	C	P/M		R																												
			9H-CC	80.9	C	P/M																														
		1.00	10H-CC	90.4	C	M						R					R																	T		
Quaternary			11X-CC	99.1	A	M	Oceanic				T			R																				R		
			12X-CC	108.7	F	P/M	Coastal					R		R															T			R				
			13X-CC	118.3	A	M											F				R				R		R									
			14X-CC	128.0	R	P				T													T							T						
			15X-CC	137.7	A	M/G			R																R											
			16X-CC	147.3	A	M/G		R								R																		R		
			17X-CC	156.9	F	P	Upwelling							T														T						T	T	
	NPD 10		18X-CC	176.1	A	M/G	Upwelling					T		T									R											T		
			19X-CC	176.1	A	M	Upwelling																														
		1.58	20X-CC	185.7	A	M/G								T																						
			21X-CC	195.3	A	P		R				R																								
			22X-CC	204.9	A	P	Upwelling					R												R												
			23X-CC	214.5	C	M																												R		
			24X-CC	224.2	C	P	Upwelling			R	R		R						R							R								R		
		2.00	25X-CC	233.8	A	P/M																												R		
			26X-CC	243.5	A	M/G	Upwelling											R																		
			27X-CC	253.0	A	P/M	Upwelling																	R												
			28X-CC	262.5	C	P															R															
			29X-CC	272.2	A	P/M		R													R															
			30X-CC	281.8	A	P/M																												F		
			31X-CC	291.5	C	P/M					R												R													
		2.40	32X-CC	301.1	A	P/M		R															C													R
			33X-CC	310.7	A	P/M																	R													
			34X-CC	320.3	C	P/M																														
	NPD 9		35X-CC	330.0	A	P																														
late Pliocene			36X-CC	339.7	A	M	Coastal					R						R	R				R													
			37X-CC	349.4	C	P																	R										R			
			38X-CC	359.0	C	P/M																	R			R										
			39X-CC	368.7	C	M																		R											R	
			40X-CC	378.3	F	P							R				R					R	R													
			41X-CC	387.9	C	P/M												R					R								R					
			42X-CC	397.5	F	P/M															R		R													
			43X-CC	407.0	C	P/M																												R		
		2.70	44X-CC	416.7	F	P									R								R											R		
	NPD 8		45X-CC	426.2	F	P/M																	F											R		F

Note: See “Explanatory Notes” chapter for abbreviations.

Table 6 (continued).

Geologic age	North Pacific diatom zone	Numeric age (Ma)	Core, section, interval	Sample depth (mbsf)	Group abundance	Preservation	Environment	*Neodenticula koizumii*	*Neodenticula* cf. *koizumii*	*Neodenticula seminae*	*Neodenticula* cf. *seminae*	*Neodenticula seminae* (sensu Akiba)	*Nitzschia fossilis*	*Nitzschia granulata*	*Nitzschia marina*	*Nitzschia reinholdii*	*Nitzschia* sp.	*Paralia sulcata*	*Pseudoeunotia doliolus*	*Rhaphoneis* sp.	*Rhizosolenia barboi*	*Rhizosolenia curvirostris*	*Rhopalodia* sp.	*Stephanopyxis turris*	*Thalassionema nitzschioides*	*Thalassionema nitzschioides parva*	*Thalassiosira antiqua*	*Thalassiosira convexa*	*Thalassiosira eccentrica*	*Thalassiosira leptopus*	*Thalassiosira oestrupii*	*Thalassiosira* spp.	*Thalassiothrix longissima*	*Thalassiothrix* spp.	Diatom fragments (girdle bands)	Spore of diatoms	Sponge spicules
		0.00	167-1018A- 1H-CC	4.9	F	P	Coastal			T														C	R							F				R
			2H-CC	14.4	C	P/M				R													R	C	R				R								T
			3H-CC	23.9	F	P												F						C	F												C
	NPD 12		4H-CC	33.4	C	M	Coastal																	C									R				F
			5H-CC	42.9	F	M				T														C													
			6H-CC	52.4	R	P/M																		T													
		0.30	7H-CC	61.9	C	P/M	Coastal			F														R		T										
			8H-CC	71.4	C	P/M				C					R				R			F		C	R					R			F			
	NPD 11		9H-CC	80.9	C	P/M				R												C		F												R
		1.00	10H-CC	90.4	C	M				C					R				R			F											F			
Quaternary			11X-CC	99.1	A	M	Oceanic			C					R				R		R	F		F					R				F	C		
			12X-CC	108.7	F	P/M	Coastal			F														C	R										P	
			13X-CC	118.3	A	M				C					R	R			R		R			C									R			
			14X-CC	128.0	R	P				T							T		T					T	T											
			15X-CC	137.7	A	M/G				A					R	R					R	F		A									R			F	
			16X-CC	147.3	A	M/G				A										R		F		A									R			F	
			17X-CC	156.9	F	P	Upwelling			C														C											A		
	NPD 10		18X-CC	176.1	A	M/G	Upwelling			C		T			T						T	F										R	F	A			
			19X-CC	176.1	A	M	Upwelling			R											R	R		F							R				A		
		1.58	20X-CC	185.7	A	M/G				C												R		F													
			21X-CC	195.3	A	P				F											R			F											A		
			22X-CC	204.9	A	P	Upwelling			F											R														A		
			23X-CC	214.5	C	M				C					R	R					F			R	R								R				
			24X-CC	224.2	C	P	Upwelling			R		R												F											A		
		2.00	25X-CC	233.8	A	P/M				C					R		R				F										R						
			26X-CC	243.5	A	M/G	Upwelling	R		A								R			F			R													
			27X-CC	253.0	A	P/M	Upwelling	R		A						R					F																
			28X-CC	262.5	C	P				R						R					R			F									R				
			29X-CC	272.2	A	P/M		F		C		F									R									R						
			30X-CC	281.8	A	P/M		F		F											C																
		2.40	31X-CC	291.5	C	P/M				F			R			R					R			F													
			32X-CC	301.1	A	P/M		F		F											F			F				F		R							
			33X-CC	310.7	A	P/M		F		F						R					R			F									R				
			34X-CC	320.3	C	P/M		F													C			A				R									
	NPD 9		35X-CC	330.0	A	P		F		T											C			F									F	C			
late Pliocene			36X-CC	339.7	A	M	Coastal		R	R			R								R			R													
			37X-CC	349.4	C	P		R													R		R	R				R									
			38X-CC	359.0	C	P/M							R								R			R									R				
			39X-CC	368.7	C	M		R	R							R					R			R						R						
			40X-CC	378.3	F	P		R		R							R				R							R			R		R			
			41X-CC	387.9	C	P/M		R																F						R			F				
			42X-CC	397.5	F	P/M		R						R							R																
			43X-CC	407.0	C	P/M															R			R									R				
		2.70	44X-CC	416.7	F	P		R											R		R		R	R			R	R			R						
	NPD 8		45X-CC	426.2	F	P/M		R			R										F			F							F						

Table 7. Distribution and relative abundance of diatoms in Holes 1018B and 1018C.

Geologic age	North Pacific diatom zone	Numeric age (Ma)	Core, section, interval	Sample depth (mbsf)	Abundance	Preservation	Environment	*Actinocyclus curvatulus*	*Actinocyclus oculatus*	*Actinoptychus senarius*	*Aulacosira granulata*	*Biddulphia aurita*	*Cocconeis costata*	*Cocconeis pellucida*	*Cocconeis* sp.	*Coscinodiscus oculus iridis*	*Coscinodiscus radiatus*	*Coscinodiscus* sp.	*Cymbella* sp.	*Denticulopsis hustedtii*	*Denticulopsis hyalina*	*Grammatophora* sp.	*Hemidiscus cuneiformis*	*Navicula* spp.	*Neodenticula koizumii*
			167-1018B-																						
			1H-CC	6.5	C	P/M												R							
			2H-CC	19.2	A	M		F								R									
			167-1018C-																						
		0.00	1H-CC	6.5	R	P							R												
			2H-CC	16.0	C	M		R																	
	NPD 12		3H-CC	25.5	R	P																			
			4H-CC	35.0	F	P/M																			
			5H-CC	44.5	T	P																			
			6H-CC	54.0	T	P														T					
			7H-CC	63.5	T	P														T					
		0.30	8H-CC	69.5	T	P																T			
			9H-CC	79.0	F	P																			
			10H-CC	88.5	F	P/M																			
			11X-CC	98.2	A	P/M							R												
			12X-CC	107.9	R	P						T		R											
Quaternary			13X-CC	117.5	F	P	Upwelling																		
	NPD 11		14X-CC	127.2	A	M/G	Upwelling																		
		1.04	15X-CC	52.6	A	M/G	Upwelling	R										R							
			16X-CC	146.6	A	M/G	Upwelling			R															
		1.12	17X-CC	156.3	F	P										F	F								
			18X-CC	165.9	A	P/M	Upwelling					R			R				R			R			
			19X-CC	175.5	C	P/M	Upwelling	R					R												
		1.58	20X-CC	185.2	A	M/G	Upwelling																		
			21X-CC	194.7	A	M/G	Upwelling	F					R				R								
			22X-CC	204.4	A	M/G																			
	NPD 10		23X-CC	214.0	C	P/M																	R		
			24X-CC	223.6	C	P/M			R																
		2.00	25X-CC	233.3	C	M		R															R		
			26X-CC	242.9	A	M/G																		R	F
late Pliocene	NPD 9		27X-CC	252.5	A	M																			F
			28X-CC	262.2	C	P																			

Note: See “Explanatory Notes” chapter for abbreviations.

posite depths were aligned so that tie points between adjacent holes occurred at exactly the same depths in meters composite depth. Intervals having significant disturbance or distortion were avoided if possible. The Site 1018 splice (Table 13, also on CD-ROM, back pocket) can be used as a sampling guide to recover a single continuous sedimentary sequence down to 193 mcd.

A preliminary age model (Table 14) was constructed to estimate sedimentation rates (Fig. 15). The age model was applied to the spliced records of GRAPE, magnetic susceptibility, and color reflectance shown in Figure 16.

INORGANIC GEOCHEMISTRY

We collected 18 interstitial water samples from Hole 1018A at depths ranging from 2.95 to 401.95 mbsf, with samples covering the two lithostratigraphic units defined at this site (see “Lithostratigraphy” section, this chapter). Chemical gradients in the interstitial waters at this site (Table 15) reflect organic matter diagenesis, the dissolution of biogenic opal and calcium carbonate, the influence of authigenic mineral precipitation, and the diffusive influence of reactions in the underlying basalt.

Chlorinity ranges from 553 to 561 mM from 2.95 to 75.85 mbsf, then decreases by 1.9% on average to a mean value of 547 mM from 103.55 to 401.95 mbsf (Fig. 17). Salinity, measured refractively as total dissolved solids, ranges from 31 to 35.5, showing a pattern similar to the chloride profile of higher salinities in the upper sediment section. Sodium concentrations measured by flame emission spectrophotometry were on average <1% lower than those estimated by charge balance (Table 15).

Alkalinity increases to peak values >50 mM from 18.85 to 75.85 mbsf, a depth range corresponding to lithostratigraphic Subunit IA, then decreases steeply and consistently with depth to 11.2 mM at 401.95 mbsf (Fig. 17). Sulfate concentrations decrease to values below the detection limit (~1.3 mM) by 9.35 mbsf. Phosphate concentrations increase to maximum values >165 µM from 18.85 to 47.35 mbsf, with a peak value of 182 µM at 37.85 mbsf, with these maximum phosphate concentrations in lithostratigraphic Subunit IA coincident with maximum alkalinity values. Phosphate concentrations then decrease with increasing depth, with a steep decline to values of 100–110 µM in the two samples from 75.85 to 103.85 mbsf, then increasingly more gradual declines to 14 µM at 257.45 mbsf and to 5–6 µM in the two deepest samples from 373.15 to 401.95 mbsf. Ammonium concentrations increase with increasing depth between >6.5 mM and 7.5 mM from 103.55 to 257.45 mbsf, then decline to values of 4.7 to 4.8 mM in the two deepest samples from 373.15–401.95 mbsf.

Dissolved silicate concentrations increase with depth, at first rapidly, then more gradually, to values >1000 µM from 286.25 to 401.95 mbsf (Fig. 17), indicative of the dissolution of biogenic opal. Strontium concentrations increase with depth from seawater values at 2.95 mbsf to 269 µM at 401.95 mbsf, consistent with the influence of the dissolution and/or recrystallization of calcium carbonate.

Calcium concentrations decrease to a minimum of 3.6 mM at 28.35 mbsf, then increase with increasing depth to 11.5 mM in the

Table 7 (continued).

Geologic age	North Pacific diatom zone	Numeric age (Ma)	Core, section, interval	Sample depth (mbsf)	Group abundance	Preservation	Environment	*Neodenticula seminae*	*Neodenticula* cf. *seminae*	*Neodenticula seminae* (sensu Akiba)	*Nitzschia marina*	*Nitzschia reinholdii*	*Paralia sulcata*	*Rhaphoneis surirella*	*Rhizosolenia barboi*	*Simonseniella (Rhizosolenia) curvirostris*	*Rhizosolenia matuyamai*	*Stephanopyxis turris*	*Stephanopyxis* sp.	*Thalassionema nitzschioides*	*Thalassiosira oestrupii*	*Thalassiothrix longissima*	*Thalassiothrix* spp.	Diatom fragments (girdle bands)	Spores of diatoms
			167-1018B-																						
			1H-CC	6.5	C	P/M												R		R	R			R	
			2H-CC	19.2	A	M							R					C					A	A	
			167-1018C-																						
		0.00	1H-CC	6.5	R	P			R									F							
			2H-CC	16.0	C	M								R				A					F	C	
			3H-CC	25.5	R	P								R				F							
	NPD 12		4H-CC	35.0	F	P/M												A					R		
			5H-CC	44.5	T	P												R							
			6H-CC	54.0	T	P																			
			7H-CC	63.5	T	P																			
		0.30	8H-CC	69.5	T	P												R							
			9H-CC	79.0	F	P					R					R		C		R				A	
	NPD 11		10H-CC	88.5	F	P/M		F							F	F									
			11X-CC	98.2	A	P/M		A								R		R							
			12X-CC	107.9	R	P		R										C							
Quaternary			13X-CC	117.5	F	P	Upwelling	F					R					F			R			A	
			14X-CC	127.2	A	M/G	Upwelling	A				R				F		F				R		A	
		1.04	15X-CC	52.6	A	M/G	Upwelling	A			R	R				R								A	
			16X-CC	146.6	A	M/G	Upwelling	C			R				F	F	F						A	A	
		1.12	17X-CC	156.3	F	P		F				R				R		F							
			18X-CC	165.9	A	P/M	Upwelling	F								R		C						A	
			19X-CC	175.5	C	P/M	Upwelling	R										C						A	
		1.58	20X-CC	185.2	A	M/G	Upwelling	A			R				R	R		C		R					A
			21X-CC	194.7	A	M/G	Upwelling	F							R			F						A	F
			22X-CC	204.4	A	M/G		F										C	R					C	
	NPD 10		23X-CC	214.0	C	P/M		C			R				R			F				R			
			24X-CC	223.6	C	P-M		F							R			R						A	
		2.00	25X-CC	233.3	C	M		C				F			R			R		R					
			26X-CC	242.9	A	M/G		C		F		R						F							
late Pliocene	NPD 9		27X-CC	252.5	A	M		F							F						R		A	A	
			28X-CC	262.2	C	P		R				R			F			R				R			

Table 8. Diatom events in Holes 1018A, 1018C, and 1018D.

Event	Age (Ma)	Hole 1018A	Depth (mbsf)	Hole 1018C	Depth (mbsf)	Hole 1018D	Depth (mbsf)
LO *S. curvirostris*	0.30	7H-CC/8H-CC	61.9/71.4	8H-CC/9H-CC	69.5/79.0	7H-CC/8H-CC	66.3/75.8
LO *R. matuyamai*	0.91–1.04	Not found	—	15X-CC/16X-CC	136.9/146.6	Not found	—
FO *R. matuyamai*	0.98–1.12	Not found	—	16X-CC/17X-CC	146.6/156.3	Not found	—
LCO *A. oculatus*	1.00–1.44	10H-CC/11X-CC	90.4/99.10	Not found	—	Not found	—
FO *S. curvirostris*	1.58	20X-CC/21X-CC	185.7/195.3	20X-CC/21X-CC	185.2/194.7	Not found	—
LO *N. koizumii*	2.00	25X-CC/26X-CC	233.8/243.5	25X-CC/26X-CC	233.3/242.9	Not found	—
LO *T. convexa*	2.40	31X-CC/32X-CC	291.5/301.1	Not found	—	Not found	—
LCO *N. kamtschatica*	2.63–2.70	44X-CC/45X-CC	416.7/426.2	Not found	—	Not found	—

Note: LO = last occurrence, FO = first occurrence, LCO = last common occurrence.

deepest sample at 401.95 mbsf (Fig. 17). Magnesium concentrations generally decrease throughout the section from 51.2 mM at 2.95 mbsf to 22.0 mM at 401.95 mbsf, with a suggestion of a slight decrease in the sample at 9.35 mbsf corresponding to a major calcium decrease and alkalinity increase. The decrease in dissolved calcium in the upper sediment indicates that authigenic mineral precipitation is significant in influencing the Ca profile in this depth range, while the magnesium profile appears dominated by the diffusive influence of reactions in underlying basalt. At depths ≥75.85 mbsf, the depth of the calcium minimum, the calcium increase is linearly correlated to the magnesium decrease, with $\Delta Ca/\Delta Mg$ of –0.28 ($R^2 = 0.97$). Potassium concentrations generally decrease with increasing depth to values around 8.5 mM from 286.25 to 401.95 mbsf (Table 15). Lithium concentrations are below typical seawater values in lithostratigraphic Subunit IA from 2.95 to 47.35 mbsf, then increase with increasing depth to 141 µM at 401.95 mbsf (Fig. 17).

ORGANIC GEOCHEMISTRY

We conducted measurements of elemental composition and volatile hydrocarbons in sediments from Site 1018 (for methods see "Organic Geochemistry" section, "Explanatory Notes" chapter, this volume).

Table 9. Distribution and relative abundances of radiolarians in Hole 1018A.

Zone	Core, section, interval	Depth (mbsf)	Abundance	Preservation	*Acrosphaera murrayana*	*Actinoma delicatulum*	*Actinomma popofski*	*Amphimelissa setosa*	*Anthocyrtidium nosicaae*	*Anthocyrtidium pliocenica*	*Botryostrobus aquilonaris*	*Botryostrobus praetumidulus*	*Botryostrobus tumidulus*	*Ceratospyris hyperborea*	*Circodiscus ellipticus*	*Clathrocyclas bicornis*	*Clathrocyclas bicincta*	*Cycladophora bicincta*	*Cycladophora craspedota*	*Cycladophora davisiana davisiana*	*Dictyophimus crisiae*	*Dictyophimus infabricatus*	*Eucyrtidium acuminatum*	*Eucyrtidium calvertense*	*Eucyrtidium erythromystax*	*Eucyrtidium infundibulum*	*Eucyrtidium matuyamai*	*Eucyrtidium teuscheri*	*Gondwanaria dogeli*	*Lamprocyclas hadros*	*Lamprocyclas junonis*	*Lamprocyrtis daniellae*	*Lamprocyrtis heteroporos*
	167-1018A-																																
	1H-CC	4.9	F	G			R				R		R					C		C	R												
	2H-CC	14.4	A	G										F				A	R	A	F				T			T					
B. aquilonaris	3H-CC	23.9	A	G			R				T			A				A	C	A	F								R		T		
	4H-CC	33.4	C	G		C	F						R	A				A		A	R										R		
	5H-CC	42.9	A	G		R	C	R			R			A				A	R	A	C							R	T				
	6H-CC	52.4	F	M		R	R				F		F					R		F	R												
	7H-CC	61.9	A	G	T		A				C		C					A		A	C	T		C		T				R			
	8H-CC	71.4	A	G		R		T					R	C				A		A	F							R	T				
	9H-CC	80.9	A	G	T		R				R							C		A	R					T							
	10H-CC	90.9	A	G							F		F					A	R	A	C	T		R		T		T	T		R		
S. universus	11X-CC	99.1	A	G	T		R				C		F					A	R	A	F			T				R			R		
	12X-CC	108.7	F	M							R			R				R		R	R								R				
	13X-CC	118.3	A	G	R		C	R			A			C				A		A	F							R	R				
	14X-CC	128.0	F	M			A				A							A		C	F												
	15X-CC	137.7	A	G			C				C		C	R		R		A	R	A	F							R	R		F		
	16X-CC	147.3	A	G			C				F		F	R		A		R		A	C							R					
	17X-CC	156.9	A	G			C				F		A	R		F		F		A	F						R	R					
	18X-CC	166.5	A	G					T		R	R				C			T	A	R						R		T		R		
	19X-CC	176.1	A	G			F				F			A		A				A							R	R	T		F		
	20X-CC	185.7	A	G										C		A			T	A							R						
	21X-CC	195.3	A	G			F		R				T	C		A				A							R	T			R		R
E. matuyamai	22X-CC	204.9	A	G			A					C	R	C		A				A							R						C
	23X-CC	214.5	A	G							F	C		F	R	A				A	R						F		T				A
	24X-CC	224.2	C	G			R							C		C				A	F						R						C
	25X-CC	233.8	A	G			A				A	A				A				A	R			R			R		T	T			A
	26X-CC	243.5	A	G			C					A		A		A				A			T	R			R						C
	27X-CC	253.0	A	G		R	A					A								A					R		R	R	R		F		A
	28X-CC	262.5	A	G			R					A		F		A				A	R						R	R					A
	29X-CC	272.2	A	G			C				C	C		R		A			R	A	R				T								A
	30X-CC	281.8	C	G												A				A						T							A
	31X-CC	291.5	C	G			C				R			R		A			R	A	R				T			T	T				A
	32X-CC	301.1	A	G			R					R				C				C	F			T				T			R		A
	33X-CC	310.7	F	G			R				R	R		R	T					C	R			T				R					
	34X-CC	320.3	A	G																R									T				A
	35X-CC	330.0	A	G			A					C				C				T	C				T				T			F	A
S. langii	36X-CC	339.7	A	G			C									C					F		T	R							T		A
	37X-CC	349.4	A	G								R		R		A					R							T					A
	38X-CC	359.0	C	G							R	F				A			T									R					A
	39X-CC	368.7	C	G								A							T														A
	40X-CC	378.3	C	G			R			T						A					R			R		T		R					A
	41X-CC	387.9	F	G			R									C			T										R				A
	42X-CC	397.5	F	G												C								R				R					A
	43X-CC	407.0	F	M								F			R	F								F		T							A
	44X-CC	416.7	A	G			R			R		A				A							T	R	R			R	T	R			A
	45X-CC	426.2	A	G			R					R				R										T		R			R		A

Note: See “Explanatory Notes” chapter for abbreviations.

Table 9 (continued).

Zone	Core, section, interval	Depth (mbsf)	Abundance	Preservation	*Lamprocyrtis neoheteroporos*	*Lamprocyrtis nigriniae*	*Lipmanella virchowii*	*Lithostrobus hexagonalis*	*Lychnocanoma n. sakai*	*Phormostichoartus crustula*	*Phormostichoartus multiseriatus*	*Plectacantha cresmatoplegma*	*Pseudocubus warreni*	*Pterocanium auritum*	*Pterocanium korotnevi*	*Pterocorys clausus*	*Pterocorys minythorax*	*Pterocorys zancleus*	*Rhizosphaera antarctica*	*Rhopalastrum profunda*	*Siphocampe arachnea*	*Siphostichoartus scalaris*	*Sphaeropyle langii*	*Sphaeropyle robusta*	*Spongotrochus glacialis*	*Stichocorys peregrina*	*Stylacontarium acquilonium*	*Stylatractus universus*	*Stylochlamidium venustum*	*Stylodictya validispina*
B. aquilonaris	167-1018A-																													
	1H-CC	4.9	F	G		R									C				R				R							R
	2H-CC	14.4	A	G		R	T		R			R			A	A			R	R		F	R		F					R
	3H-CC	23.9	A	G			F							R	A	A						R	F		F				T	R
	4H-CC	33.4	C	G			R		A					R	A	C		R					R		R		T		R	R
	5H-CC	42.9	A	G		C			C				T		A	C			R	R		R	C		F		R		R	C
	6H-CC	52.4	F	M					R																					
S. universus	7H-CC	61.9	A	G		A	T	R	F	F				R	A	A	T		R				F		F		C			C
	8H-CC	71.4	A	G		A	F		A	R	R		R	F	C	R							A						F	F
	9H-CC	80.9	A	G		A	T						T		C	F		T		T		R	C				R	R	T	
	10H-CC	90.9	A	G		A			F			T				A		R	R	R			R				R	R		F
	11X-CC	99.1	A	G	R	A		R			T			F	R	A			F	F			A				A	F		R
	12X-CC	108.7	F	M												R									R			R		
	13X-CC	118.3	A	G	C	A	R		C		R					F			R			R	C		C		C	C		R
	14X-CC	128.0	F	M												R			R	R			F		R		F	T		R
	15X-CC	137.7	A	G	R		R		R						F	C			F	R					R			R		
	16X-CC	147.3	A	G	R									T		R						T	R		R					
E. matuyamai	17X-CC	156.9	A	G	C				R						R								R		R			R		R
	18X-CC	166.5	A	G	A		R		R						F	F						R	R		T		R	F		
	19X-CC	176.1	A	G										R								R	R		R		R	R		
	20X-CC	185.7	A	G	A				R			T		R		R						R	R					R		R
	21X-CC	195.3	A	G	R									R											R		R	C	R	R
	22X-CC	204.9	A	G	R		R				R			R									R	R	R			C		R
	23X-CC	214.5	A	G	C		R						R		R				R	R		R	R		R		R	C		F
	24X-CC	224.2	C	G	F		R		R				R			R									R		F	R		R
	25X-CC	233.8	A	G					R				C	R	R	R				R		R	C				R	F		
	26X-CC	243.5	A	G	C		R			T			R		R								C					R		R
	27X-CC	253.0	A	G	F		R		R		T			C						R			R				F	F		T
	28X-CC	262.5	A	G	R								R	T						R			R				F	C		R
S. langii	29X-CC	272.2	A	G	C				R		R		R	R									R					C		
	30X-CC	281.8	C	G	F						T		R							R		T	R							R
	31X-CC	291.5	C	G						T	C		R	T									R							
	32X-CC	301.1	A	G	R					R	C		F	R					F			R	R					T		F
	33X-CC	310.7	F	G	T						F		R	R					R									R		
	34X-CC	320.3	A	G											R										T			R		
	35X-CC	330.0	A	G					R		R		F	R	F					R							R	F		R
	36X-CC	339.7	A	G							R		F	R	F				F	R							F	R		
	37X-CC	349.4	A	G									R												T	R	R	R		
	38X-CC	359.0	C	G					T				R						R								T			R
	39X-CC	368.7	C	G				T	R		R		R						R											R
	40X-CC	378.3	C	G					T		R		R													T	R	R		
	41X-CC	387.9	F	G					R				R																	R
	42X-CC	397.5	F	G					R		R				R												F	F		R
	43X-CC	407.0	F	M											R													R		R
	44X-CC	416.7	A	G						T			T													R		R		
	45X-CC	426.2	A	G						T														R			R	F		

Table 10. Radiolarian events in Holes 1018A, 1018C, and 1018D.

		Hole 1018A		Hole 1018C		Hole 1018D	
Label	Event	Top (mbsf)	Bottom (mbsf)	Top (mbsf)	Bottom (mbsf)	Top (mbsf)	Bottom (mbsf)
R1	LO *S. acquilonium*	23.9	33.4	16.0	25.5	18.8	28.3
R2	LO *S. universus*	71.4	80.9	?	79.0	?	?
R3	LO *L. neoheteroporos*	90.9	99.1	88.5	98.2	66.3	75.8
R4	FO *L. nigriniae*	118.3	128.0	127.2	136.9	110.1	119.7
R5	LO *E. matuyamai*	147.3	156.9	136.9	146.6	138.9	148.5
R6	LO *L. heteroporos*	185.7	195.3	175.5	185.2		
R7	FO *E. matuyamai*	265.5	272.2	262.2	?		
R8	FO *L. neoheteroporos*	310.7	320.3				
R9	FO *C. d. davisiana*	330.0	339.7				
R10	LO *S. peregrina*	339.7	349.4				
R11	LO *A. pliocenica*	368.7	378.3				

Note: LO = last occurrence, FO = first occurrence.

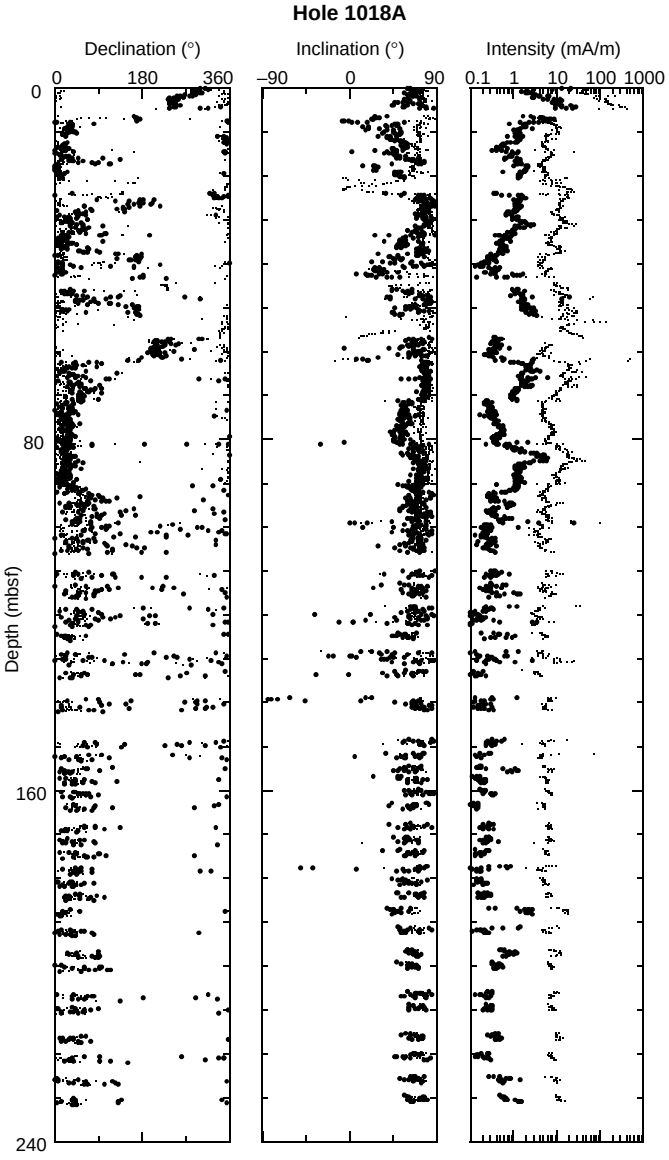

Figure 10. Plots of magnetic declination, inclination, and intensity of APC (0–90 mbsf) and XCB (90–230 mbsf) cores from Hole 1018A. Small and large dots represent the data before and after AF demagnetization at 20 mT, respectively.

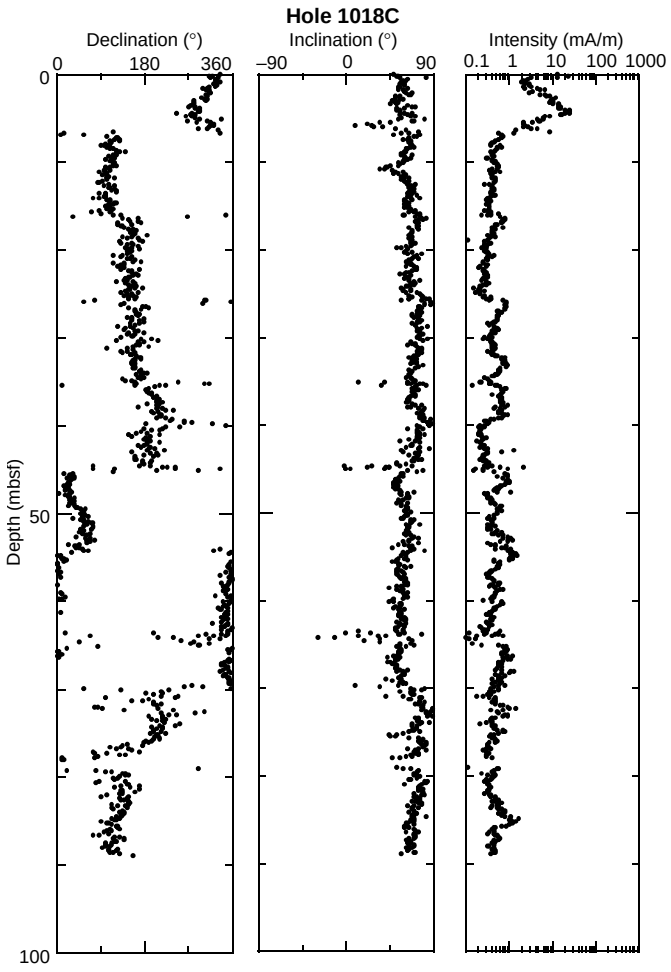

Figure 11. Plots of magnetic declination, inclination, and intensity of APC cores from Hole 1018C after AF treatment at 20 mT.

Volatile Hydrocarbons

The concentrations of methane, ethane, and propane were routinely monitored in Hole 1018A because of shipboard safety and pollution prevention considerations. The results are displayed in Figure 18 and Table 16. Headspace methane concentration increases to 60,000 ppm within the uppermost 28 mbsf. Below 28 mbsf, the concentration is constantly high with little fluctuation. Some higher amounts of ethane were recorded (2–13 ppm) in the lowermost part of this hole. Methane/ethane ratios show a gradual decrease from top to bottom of the hole, but never reach values below 1,600 (Fig. 18). No indications for migrated gas could be found. The first obvious gas voids occurred

Table 11. Stepwise AF demagnetization of single specimens from Hole 1018A.

Sample	AF (mT)	Declination (°)	Inclination (°)	Intensity (mA/m)
167-1018A-				
11X-2, 92–94 cm	0	331.4	72.6	1.29
	5	337.8	50.8	0.42
	10	321.1	49.8	0.24
11X-6, 70–72 cm	0	22.2	80.9	1.63
	5	40.7	65.3	0.55
	10	44.9	64.1	0.45
	15	45.2	61.0	0.32
12X-2, 13–15 cm	0	211.6	85.9	1.03
	5	186.1	73.3	0.29
	10	192.5	62.3	0.20
12X-5, 42–44 cm	0	352.9	82.3	1.40
	5	42.6	78.1	0.47
	10	53.4	60.2	0.30
13X-4, 62–64 cm	0	143.1	86.7	1.42
	0	164.2	83.3	1.18
	10	111.8	68.0	0.18
	20	153.4	54.9	0.18
13X-3, 53–55 cm	0	124.1	81.5	2.39
	5	129.1	64.9	0.59
	10	133.5	55.6	0.37
	15	130.7	47.9	0.31
14X-1, 42–44 cm	0	323.8	83.9	1.31
	5	190.7	83.7	0.37
	10	177.4	74.1	0.20
14X-7, 43–45 cm	0	302.2	82.3	1.16
	0.5	291.5	83.7	1.13
	2.5	274.3	84.1	0.97
	5	271.0	76.9	0.20
	10	177.6	2.4	0.60
15X-3, 14–16 cm	0	338.7	84.7	1.42
	2.5	244.5	85.6	0.75
	5	81.8	82.4	0.22
	7.5	171.3	57.3	0.11
	10	144.2	54.4	0.38
15X-7, 13–15 cm	0	231.6	85.9	1.25
	2.5	201.3	82.6	0.85
	5	233.8	73.6	0.27
	7.5	242.3	47.4	0.18
	10	255.4	28.6	0.15
	15	260.7	18.1	0.11

at about 19 mbsf and vacutainer samples were taken whenever voids were observed on the catwalk.

Elemental Analysis

At Site 1018, 156 sediment samples were analyzed for total carbon, inorganic carbon, total nitrogen, and total sulfur. Results are presented in Table 17 (also on CD-ROM, back pocket) and Figure 19.

The percentage of calcium carbonate ($CaCO_3$) was calculated from the inorganic carbon concentrations by assuming that all carbonate occurs in the form of calcite. In the upper 350 mbsf, the average $CaCO_3$ concentration is ~3 wt%. A few samples reached up to 16 wt% carbonate, which likely reflect, interbedded nannofossil-rich strata (see "Lithostratigraphy" section, this chapter). Below 350 mbsf (~2.8 Ma) the carbonate content increases to an average of 15 wt%, showing a high-amplitude fluctuation between 5 and 25 wt%. This transition corresponds to a distinct lithologic change from diatom clay to clayey nannofossil chalk.

The total organic carbon (TOC) content varies between 0.5 and 2.5 wt% with high amplitude fluctuation (Table 17; Fig. 19). The average value of TOC at this site is 1.3 wt%. The samples with high TOC values (>2 wt%) also display elevated total organic carbon/total nitrogen ratios, which can be attributed to a contribution of terrigenous organic matter (Table 16 in "Site 1016" chapter, this volume; Bordovskiy, 1965; Emerson and Hedges, 1988).

Total nitrogen content varies between 0.07 and 0.31 wt%, and total sulfur content ranges from 0 to ~1.91 wt% (Table 16 in "Site 1016" chapter, this volume). To characterize the type of organic matter in the sediments, TOC/TN ratios were calculated. Most of the TOC/TN ratios range between 4 and 9, which indicates a predominantly marine origin of the organic material (Bordovskiy, 1965; Emerson and Hedges, 1988).

PHYSICAL PROPERTIES

Multisensor Track Measurements

The shipboard physical properties program at Site 1018 included nondestructive measurements of bulk density, magnetic susceptibility, *P*-wave velocity, and natural gamma-ray activity on whole sections of all cores using the MST (Fig. 20). Magnetic susceptibility was measured at 4-cm intervals at low sensitivity (1-s measuring time) on all Site 1018 cores. GRAPE bulk density measurements were made at 4-cm intervals on all Site 1018 cores. PWL velocity measurements were made at 4-cm intervals on Cores 167-1018A-1H through 3H, 167-1018B-1H and 2H, and 167-1018C-1H through 5H, but were not run on cores from Hole 1018D. Natural gamma-ray activity was measured with a 15-s count every 12 cm on cores from Holes 1018A through 1018C and not run on cores from Hole 1018D.

Index Properties

Index properties measurements were made at one sample per working section on all cores from Hole 1018A. Index properties of bulk density, void ratio, porosity, water content, dry-bulk density, and grain density were determined by the gravimetric Method C (see "Physical Properties" section, "Explanatory Notes" chapter, this volume; Fig. 21; Table 18 on CD-ROM in the back pocket of this volume). Lithostratigraphic unit and subunit divisions clearly correspond with changing trends in grain density and porosity values (Fig. 22). The change from lithostratigraphic Subunit IA to Subunit IB is marked by the change in the porosity trend at approximately 75 mbsf; Subunit IA corresponds to steadily decreasing values, whereas in Subunit IB, porosity values fluctuate about a steady mean that corresponds to interbedding of diatom ooze with nannofossil ooze with diatoms. The transition from lithostratigraphic Subunit IB to Subunit IC at 201 mbsf is not reflected in any significant change in porosity. However, values of grain density drop from ~2.7 to 2.6 g/cm^3, corresponding to a decrease in the amount of nannofossils. Mean porosity and grain density values remain constant throughout lithostratigraphic Subunit IC but shift to lower and higher values, respectively, near the boundary between lithostratigraphic Units I and II (344 mbsf, see "Lithostratigraphy" section, this chapter).

Compressional Wave Velocity

No discrete *P*-wave velocity measurements were obtained at Site 1018 because the high gas content in the cores resulted in severe signal attenuation (see "Organic Geochemistry" section, this chapter).

Heat Flow

Thermal conductivity was measured to 22.65 mbsf in Hole 1018A and to 87.25 mbsf in Hole 1018C (Table 19 on CD-ROM in the back pocket of this volume). Three downhole temperature measurements were taken with the APC Adara temperature tool in Hole 1018A: 3.3°C at 52.4 mbsf, 3.8°C at 71.4 mbsf, and 4.3°C at 90.4 mbsf in Cores 167-1018A-6H, 8H, and 10H, respectively (Fig. 23). Bottom-water temperature was measured on all runs, indicating an average bottom-water temperature of 1.5°C ± 0.1°C. The four data points yield a thermal gradient of 32°C/km (Fig. 24). Using an average measured thermal conductivity of 0.847 W/(m·K) provides a heat-flow estimate of 27 mW/m^2 at Site 1018.

Color Reflectance

Reflectance measurements were made at 4- to 6-cm intervals in Holes 1018A, 1018C, and 1018D. Similar to Sites 1011 and 1016, we attempted to predict opal content using a multiple linear regression equation generated from the Leg 167 site-survey color reflectance and opal data. The equation was generated using a calibration data set

Table 12. Site 1018 composite depth section.

Core, section	Depth (mbsf)	Offset (m)	Depth (mcd)
167-1018A-			
1H-1	0.00	–0.12	–0.12
2H-1	4.90	1.04	5.94
3H-1	14.40	3.05	17.45
4H-1	23.90	4.41	28.31
5H-1	33.40	4.99	38.39
6H-1	42.90	5.55	48.45
7H-1	52.40	6.61	59.01
8H-1	61.90	7.44	69.34
9H-1	71.40	8.64	80.04
10H-1	80.90	8.94	89.84
11X-1	90.40	10.17	100.57
12X-1	99.10	10.80	109.90
13X-1	108.70	13.62	122.32
14X-1	118.30	14.05	132.35
15X-1	128.00	14.31	142.31
16X-1	137.70	14.48	152.18
17X-1	147.30	13.39	160.69
18X-2	157.22	17.41	174.63
19X-1	166.50	17.41	183.91
20X-1	176.10	16.97	193.07
21X-1	185.70	16.97	202.67
22X-1	195.30	18.47	213.77
23X-1	204.90	18.47	223.37
24X-1	214.50	18.47	232.97
25X-1	224.20	20.23	244.43
26X-1	233.80	20.23	254.03
28X-1	253.00	19.71	272.71
29X-1	262.50	19.71	282.21
30X-1	272.20	19.69	291.89
31X-1	281.80	19.69	301.49
32X-1	291.50	19.69	311.19
33X-1	301.10	19.69	320.79
34X-1	310.70	19.69	330.39
35X-1	320.30	19.69	339.99
36X-1	330.00	19.69	349.69
37X-1	339.70	19.69	359.39
38X-1	349.40	19.69	369.09
39X-1	359.00	19.69	378.69
40X-1	368.70	19.69	388.39
41X-1	378.30	19.69	397.99
42X-1	387.90	19.69	407.59
43X-1	397.50	19.69	417.19
44X-1	407.00	19.69	426.69
45X-1	416.70	19.69	436.39
167-1018B-			
1H-1	0.00	–0.18	–0.18
2H-1	9.70	–0.25	9.45

Core, section	Depth (mbsf)	Offset (m)	Depth (mcd)
167-1018C-			
1H-1	0.00	–0.08	–0.08
2H-1	6.50	0.44	6.94
3H-1	16.00	1.53	17.53
4H-1	25.50	2.25	27.75
5H-1	35.00	3.08	38.08
6H-1	44.50	3.73	48.23
7H-1	54.00	5.13	59.13
8H-1	63.50	6.30	69.80
9H-1	69.50	7.67	77.17
10H-1	79.00	9.06	88.06
11X-1	88.50	10.59	99.09
12X-1	98.20	10.79	108.99
13X-1	107.90	11.61	119.51
14X-1	117.50	12.51	130.01
15X-1	127.20	12.23	139.43
16X-1	136.90	13.55	150.45
17X-1	146.60	13.85	160.45
18X-1	156.30	15.57	171.87
19X-1	165.90	16.22	182.12
20X-1	175.50	17.88	193.38
21X-1	185.20	17.81	203.01
22X-1	194.70	19.03	213.73
23X-1	204.40	20.74	225.14
24X-1	214.00	21.04	235.04
25X-1	223.60	21.13	244.73
26X-1	233.30	21.49	254.79
27X-1	242.90	21.49	264.39
28X-1	252.50	21.49	273.99
167-1018D-			
1H-1	0.00	0.00	0.00
2H-1	9.30	0.41	9.71
3H-1	18.80	1.51	20.31
4H-1	28.30	3.11	31.41
5H-1	37.80	3.47	41.27
6H-1	47.30	3.73	51.03
7H-1	56.80	5.51	62.31
8H-1	66.30	5.27	71.57
9H-1	75.80	8.12	83.92
10H-1	85.30	8.74	94.04
11H-1	94.80	9.85	104.65
12X-1	104.30	12.03	116.33
13X-1	110.10	13.13	123.23
14X-1	119.70	13.06	132.76
15X-1	129.30	12.91	142.21
16X-1	138.90	14.67	153.57
17X-1	148.50	15.11	163.61
18X-1	158.10	16.85	174.95

Note: This table is also on CD-ROM, back pocket, this volume.

from piston core EW9504-13PC retrieved near Site 1018. These data from the interval 0–14 mbsf have an average opal content of 1.96% (by weight) and standard deviation of 0.72%. The results from the opal prediction are consistent with the major lithostratigraphic units identified by the shipboard sedimentologists at Site 1018 (Fig. 25A). In lithostratigrahic Subunit IA, which consists of clay with silt and clay with diatoms, opal is generally low, averaging 2.0%. In lithostratigraphic Subunits IB and IC, opal levels are higher (2.5% on average). Peaks in opal content match the clayey diatom ooze and diatom clay intervals, whereas lows coincide with the more clayey layers. The estimated opal levels are relatively low in nannofossil-rich lithostratigraphic Unit II, which is similar to lithostratigraphic Subunit IA.

Intervals high in predicted opal values display a spectral character similar to that of diatomaceous sediments at Site 1016. For example, diatom clay with silt (Fig. 25B) generally showed low color reflectance (<10%) and spectra with a shallow positive slope from 500 to 700 nm and a slightly greater slope from 700 to 800 nm.This is distinctly different from the spectral character of clay with silt at Site 1018 (Fig. 25C), which is also low in color reflectance (average ~11%) and displays spectra with negative slope and a broad reflectance peak centered near 550 nm. The nannofossil chalk with diatoms and clay of lithostratigraphic Unit II has spectra different from either diatom clay or clay with silt, showing a relatively flat spectrum above 500 nm and a steep positive slope from 400 to 500 nm (Fig. 25D).

Given the similarity in spectra of diatom-rich sediments at Sites 1016 and 1018, it is unclear why opal prediction at Site 1016 produced low estimated values (of order of 3%–4% for diatomites). One possible explanation is that weight percent opal is not reflected well in smear-slide percent volume estimates. At Site 1018, the frequency and relative magnitude of the estimated opal content of the sediments appear correct. However, the absolute opal content is unknown. Detailed shore-based analyses are required to evaluate the predictive capability of our opal equation.

Digital Color Video

Cores from all holes at Site 1018 were imaged with the ODP color digital imaging system at 20-cm intervals downcore, providing a 0.25-mm pixel. The intensity of color CIELAB L* from the ODP color digital imaging system from Holes 1018A, 1018C, and 1018D is shown in Figure 26.

DOWNHOLE MEASUREMENTS

Logging Operations and Log Quality

Hole 1018A was logged with only two partial passes of the density-porosity combination tool string because of poor borehole condi-

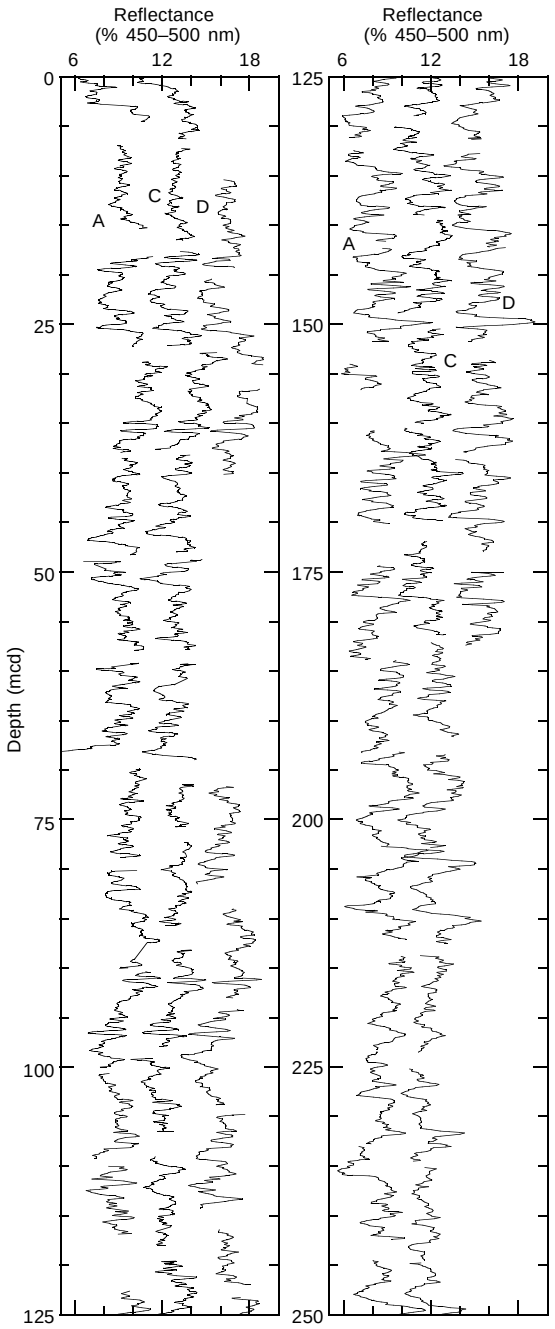

Figure 12. Smoothed (15-cm Gaussian) color reflectance (% 450–500 nm band) data for the upper 250 m from Site 1018 on the mcd scale. Holes 1018A, 1018C, and 1018D are offset from each other by a constant (5%).

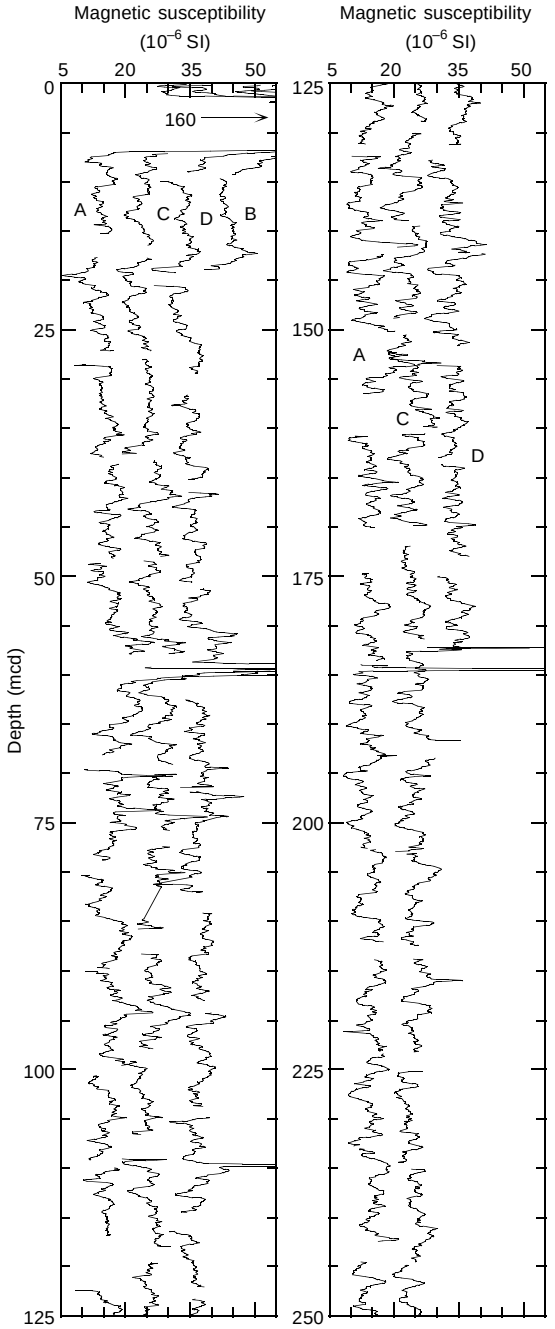

Figure 13. Smoothed (15-cm Gaussian) magnetic susceptibility data for the upper 250 m from Site 1018 on the mcd scale. Holes 1018A, 1018C, 1018D, and 1018B are offset from each other by a constant (8×10^{-6} SI).

tions. During the wiper trip, it was discovered that the hole had filled with approximately 40 m of debris. After the pipe was set at 80 mbsf (Table 20), the density-porosity combination tool string was lowered into the hole. The tool would not pass a ledge at ~222 mbsf despite repeated attempts. A partial pass of the density-porosity tool string (pass 1: 227–70 mbsf) was conducted (Fig. 27), and the tool was brought to the surface so a second complete wiper trip could be performed. Caliper measurements from pass 1 indicate that the borehole was very irregular and completely washed out (>18 in) in many places. The density-porosity combination tool was deployed again after the second wiper trip and the base of the pipe was set at 234 mbsf. The tool string would not pass an obstruction near 342 mbsf, so a second partial pass (pass 2: 342–234 mbsf; Table 20). Again, caliper measurements from pass 2 demonstrate that the borehole was very washed out. Sea-state conditions were moderately rough (2-m swells), and the wireline heave compensator was used on both passes.

Because of the poor borehole conditions, log data quality is correspondingly poor for the measurements that require good borehole contact (principally density and porosity). An example of the influence of highly variable borehole diameter on selected log measurements at Hole 1018A is shown in Figure 28; poor contact with the borehole wall produces apparent density reductions. The borehole

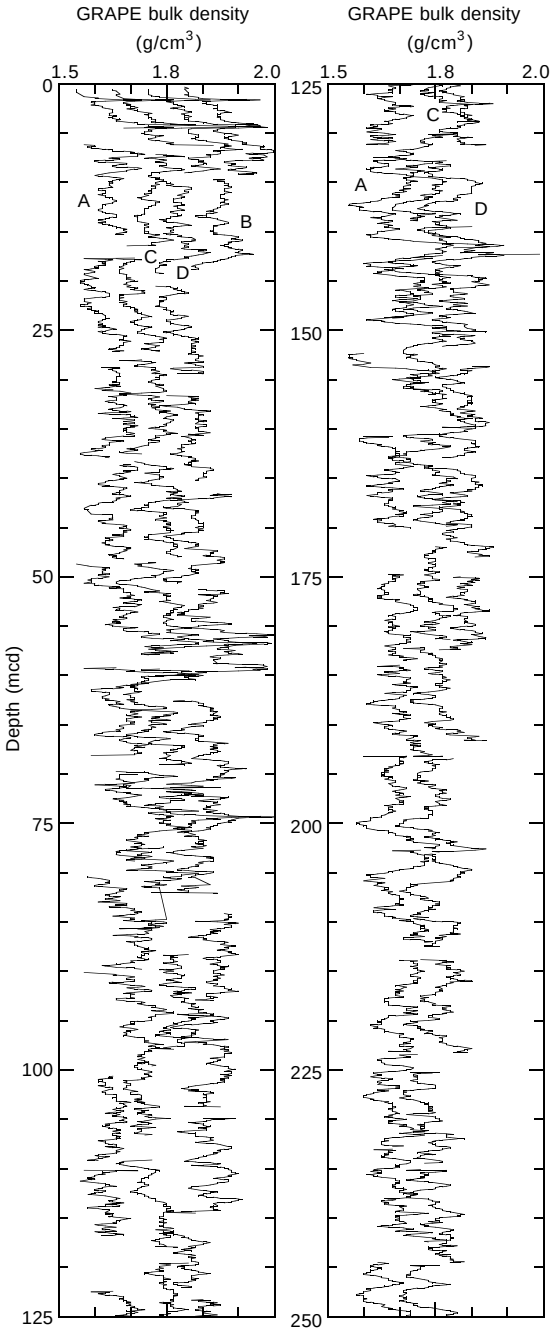

Figure 14. Smoothed (15-cm Gaussian) GRAPE bulk density data for the upper 250 m from Site 1018 on the mcd scale. Holes 1018A, 1018C, 1018D, and 1018B are offset from each other by a constant (0.1 g/cm^3).

has regular washouts at 10-m intervals, probably caused by the effects of circulation during coring (Fig. 27).

The TLT was run during pass 2 of the density-porosity combination tool string, but the measured temperatures were very low because of the excessive circulation required to drill and flush the hole.

SUMMARY

Site 1018 (Fig. 29) ties the northern Gorda Transect to the southern transects of Leg 167. It was intended to collect an upper Miocene to Holocene sediment column, but sedimentation rates were higher than anticipated. The deepest sediments recovered, at 426 mbsf, were late early Pliocene in age (~3.5 Ma) for an average sedimentation rate greater than 120 m/m.y. Four holes were drilled to 19 mbsf (~0.1 Ma), three holes to 168 mbsf (~1.3 Ma), and two holes to 262 mbsf (~2.1 Ma). The sediment column is primarily aluminosilicates in the Quaternary interval, but with higher calcium carbonate and silica microfossil content in the lower Quaternary sediments. The higher calcium carbonate in the lower (relative to upper) Quaternary sediments is consistent with the sediment columns in other relatively deep sites, that is, Sites 1016 and 1011. Site 1018 has a higher silica content than the sites within the California Borderland, but is similar to Site 1016 in this regard. The upper Pliocene sediments, unlike the borderland sites, are diatom-rich. Calcium carbonate mass accumulation rates within the upper Pliocene interval are still high, however, despite the low calcium carbonate contents.

REFERENCES

Atwater, T., and Severinghaus, J., 1989. Tectonic map of the northeast Pacific Ocean. *In* Winterer, E.L., Hussong, D.M., and Decker, R.W. (Eds.) *The Eastern Pacific Ocean and Hawaii.* Geol. Soc. Am., Decade of North Am. Geol., Vol. N.

Baldauf, J.G., and Iwai, M., 1995. Neogene diatom biostratigraphy for the eastern equatorial Pacific Ocean, Leg 138. *In* Pisias, N.G., Mayer, L.A., Janecek, T.R., Palmer-Julson, A., and van Andel., T.H. (Eds.), *Proc. ODP, Sci. Res.*, 138: College Station, TX (Ocean Drilling Program), 105–128.

Barron, J.A., and Gladenkov, A.Y., 1995. Early Miocene to Pleistocene diatom stratigraphy of Leg 145. *In* Rea, D.K., Basov, I.A., Scholl, D.W., and Allan, J.F. (Eds.), *Proc. ODP, Sci. Results*, 145: College Station, TX (Ocean Drilling Program), 3–19.

Bohannon, R.G., and Parsons, T., 1995. Tectonic implications of post-30 Ma Pacific and North American relative plate motions. *Geol. Soc. Am. Bull.*, 107:937–959.

Bordovskiy, O.K., 1965. Accumulation and transformation of organic substances in marine sediment, 2. Sources of organic matter in marine basins. *Mar. Geol.*, 3:5–31.

Emerson, S., and Hedges, J.I., 1988. Processes controlling the organic carbon content of open ocean sediments. *Paleoceanography*, 3:621–634.

Koizumi, I., 1992. Diatom biostratigraphy of the Japan Sea: Leg 127. *In* Pisciotto, K.A., Ingle, J.C., Jr., von Breymann, M.T., Barron, J., et al., *Proc. ODP, Sci. Results*, 127/128 (Pt. 1): College Station, TX (Ocean Drilling Program), 249–289.

Koizumi, I., and Tanimura, Y., 1985. Neogene diatom biostratigraphy of the middle latitude western North Pacific, Deep Sea Drilling Project Leg 86. *In* Heath, G.R., Burckle, L.H., et al., *Init. Repts. DSDP*, 86: Washington (U.S. Govt. Printing Office), 269–300.

Lyle, M., Gallaway, P.J., Liberty, L.M., Mix, A., Stott, L., Hammond, D., Gardner, J., Dean, W., and the EW9504 Scientific Party, 1995a. Data submission. W9406 and EW9504 site surveys of the California margin proposed drillsites, Leg 167 (Vol. 1): Site maps and descriptions. Boise State Univ., *CGISS Tech. Rep.*, 95–11.

————, 1995b. Data submission. W9406 and EW9504 site surveys of the California margin proposed drillsites, Leg 167 (Vol. 2): Seismic profiles. Boise State Univ., *CGISS Tech. Rep.*, 95–12.

Pratson, L., and Haxby, W., 1996. What is the slope of the U.S. continental slope? *Geology*, 24:3–6.

Savrda, C.E., Bottjer, D.J., and Gorsline, D.S., 1984. Development of a comprehensive oxygen-deficient marine biofacies model: evidence from Santa Monica, San Pedro and Santa Barbara basins, California Continental Borderland. *AAPG Bull.*, 68:1179–1192.

Ms 167IR-112

NOTE: For all sites drilled, core-description forms ("barrel sheets") and core photographs can be found in Section 3, beginning on page 499. Smear-slide data can be found in Section 4, beginning on page 1327. See Table of Contents for material contained on CD-ROM.

Table 13. Site 1018 splice tie points.

Hole, core, section, interval (cm)	Depth (mbsf)	Depth (mcd)		Hole, core, section, interval (cm)	Depth (mbsf)	Depth (mcd)
1018C-1H-4, 19	4.69	4.61	tie to	1018D-1H-4, 11	4.61	4.61
1018D-1H-6, 43	7.93	7.93	tie to	1018C-2H-1, 99	7.49	7.93
1018C-2H-7, 13	15.63	16.07	tie to	1018D-2H-5, 36	15.66	16.07
1018D-2H-6, 107	17.87	18.28	tie to	1018C-3H-1, 76	16.77	18.28
1018C-3H-6, 121	24.71	26.24	tie to	1018D-3H-4, 143	24.73	26.24
1018D-3H-6, 53	26.83	28.34	tie to	1018C-4H-1, 59	26.90	28.34
1018C-4H-6, 49	33.59	35.84	tie to	1018D-4H-3, 143	32.73	35.84
1018D-4H-5, 119	35.49	38.60	tie to	1018C-5H-1, 52	35.52	38.60
1018C-5H-5, 139	42.42	45.50	tie to	1018D-5H-3, 123	42.03	45.50
1018D-5H-7, 11	46.41	49.88	tie to	1018C-6H-2, 15	46.15	49.88
1018C-6H-6, 111	53.11	56.84	tie to	1018D-6H-4, 131	53.11	56.84
1018D-6H-6, 103	55.83	59.56	tie to	1018C-7H-1, 43	54.43	59.56
1018C-7H-6, 131	62.91	68.04	tie to	1018D-7H-4, 123	62.53	68.04
1018D-7H-7, 11	65.44	70.95	tie to	1018A-8H-2, 11	63.51	70.95
1018A-8H-7, 5	70.95	78.39	tie to	1018D-8H-5, 76	73.12	78.39
1018D-8H-6, 137	75.22	80.49	tie to	1018A-9H-1, 44	71.85	80.49
1018A-9H-5, 93	78.33	86.97	tie to	1018D-9H-3, 4	78.85	86.97
1018D-9H-5, 131	83.11	91.23	tie to	1018C-10H-3,16	82.17	91.23
1018C-10H-6, 17	86.67	95.73	tie to	1018D-10H-2, 19	86.99	95.73
1018D-10H-4, 113	90.96	99.70	tie to	1018C-11X-1, 60	89.11	99.70
1018C-11X-5, 5	94.55	105.14	tie to	1018D-11H-1, 49	95.29	105.14
1018D-11H-6, 83	103.13	112.98	tie to	1018C-12X-3,99	102.19	112.98
1018C-12X-6, 41	106.11	116.90	tie to	1018D-12X-1, 57	104.87	116.90
1018D-12X-4, 17	108.97	121.00	tie to	1018C-13X-3, 149	109.39	121.00
1018C-13X-6, 101	116.41	128.02	tie to	1018D-13X-4, 29	114.89	128.02
1018D-13X-5, 125	117.35	130.48	tie to	1018C-14X-1, 47	117.97	130.48
1018C-14X-6, 53	125.53	138.04	tie to	1018D-14X-4, 78	124.98	138.04
1018D-14X-6, 101	128.21	141.27	tie to	1018C-15X-2, 34	129.04	141.27
1018C-15X-6, 85	135.55	147.78	tie to	1018D-15X-4, 106	134.87	147.78
1018D-15X-6, 131	138.11	151.02	tie to	1018C-16X-1, 56	137.47	151.02
1018C-16X-6, 25	144.65	158.20	tie to	1018D-16X-4, 13	143.53	158.20
1018D-16X-5, 137	146.27	160.94	tie to	1018C-17X-1, 48	147.09	160.94
1018C-17X-7, 21	155.81	169.66	tie to	1018D-17X-5, 4	154.55	169.66
1018D-17X-6, 125	157.25	172.36	tie to	1018C-18X-1, 48	156.79	172.36
1018C-18X-6, 101	164.81	180.38	tie to	1018A-18X-5, 124	162.97	180.38
1018A-18X-7, 59	165.31	182.72	tie to	1018C-19X-1, 60	166.50	182.72
1018C-19X-7, 53	175.43	191.65				

Note: This table is also on CD-ROM, back pocket, this volume.

Table 14. Site 1018 sedimentation rate age control points.

Event	Depth (mcd)	Age (Ma)
T *P. lacunosa*	91.33	0.46
T *R. matuyamai*	155.30	0.98
B *G. oceanica*	227.46	1.69
T *T. convexa*	315.99	2.40
T *D. surculus*	344.84	2.61
T *D. tamalis*	373.89	2.76
T *A. pliocenica*	393.19	3.36

Note: T = top, B = bottom.

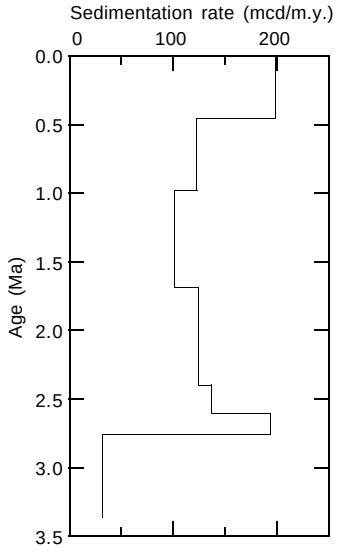

Figure 15. Sedimentation rate vs. age at Site 1018 based on the age control points from Table 14.

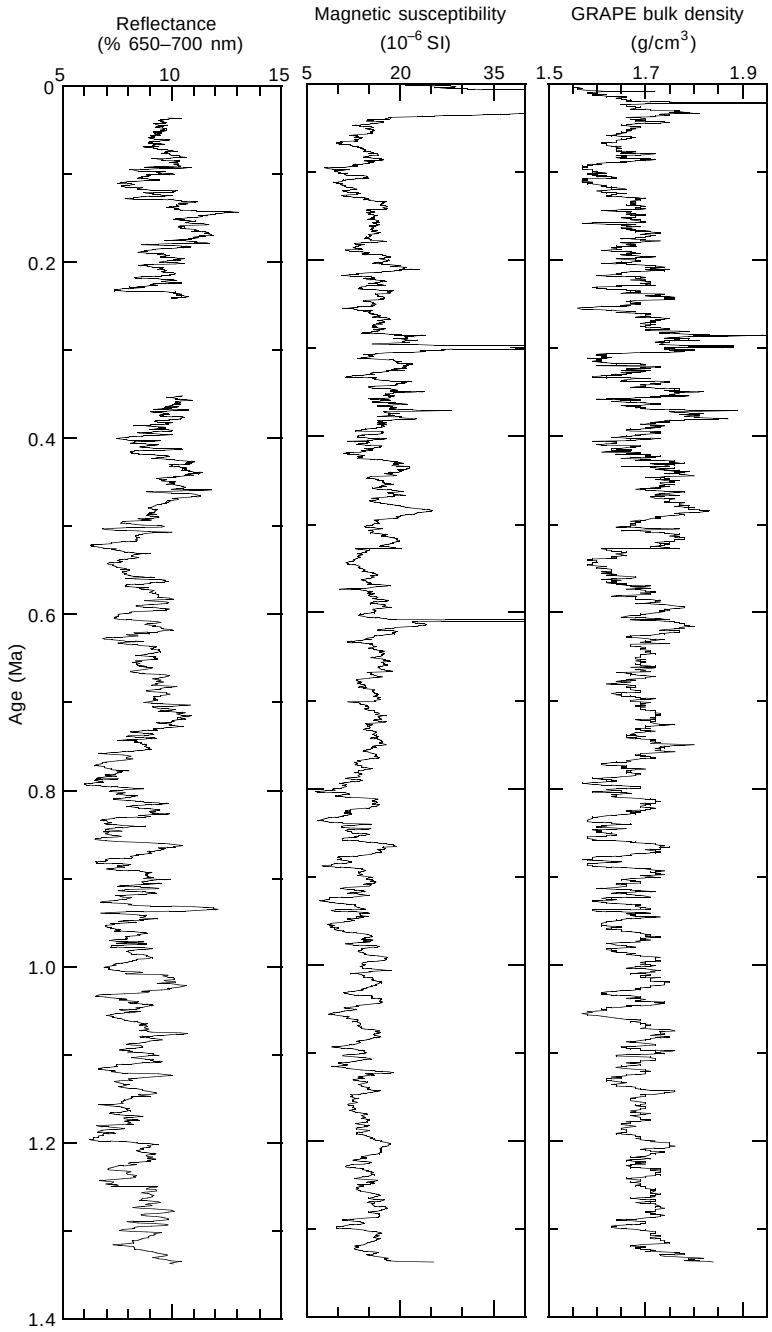

Figure 16. Spliced records of Site 1018 color reflectance, magnetic susceptibility, and GRAPE bulk density vs. age based on age control points from Table 14.

Table 15. Interstitial water geochemical data, Hole 1018A.

Core, section, interval (cm)	Depth (mbsf)	pH	Alkalinity (mM)	Salinity	Cl^- (mM)	Na^+ (mM)	SO_4^{2-} (mM)	HPO_4^{2-} (µM)	NH_4^+ (mM)	H_4SiO_4 (µM)	Ca^{2+} (mM)	Mg^{2+} (mM)	Sr^{2+} (µM)	Li^+ (µM)	K^+ (mM)
167-1018A-															
1H-2, 145–150	2.95	7.56	9.33	35.5	553	479	23.7	29	0.57	573	8.68	51.2	87	23	11.1
2H-3, 145–150	9.35	7.44	41.5	34.0	561	488	<1.3	142	2.38	750	4.21	47.9	99	13	10.7
3H-3, 145–150	18.85	7.60	50.5	35.0	559	489	<1.3	167	3.35	803	3.83	50.8	111	18	10.9
4H-3, 145–150	28.35	7.57	54.2	35.0	557	492	<1.3	165	3.93	773	3.57	50.3	119	19	11.1
5H-3, 145–150	37.85	7.50	56.3	35.0	559	497	<1.3	182	4.65	775	4.32	49.5	126	21	11.2
6H-3, 145–150	47.35	7.55	56.3	35.0	556	495	<1.3	171	4.96	816	4.39	48.5	134	24	11.3
9H-3, 145–150	75.85	7.38	51.6	34.0	557	499	<1.3	110	6.24	803	5.01	43.9	158	32	11.3
12X-3, 145–150	103.55	7.48	45.6	33.5	544	487	<1.3	100	6.94	844	6.84	39.1	182	41	10.8
16X-2, 145–150	140.65	7.42	39.3	33.0	544	484	<1.3	72	7.46	941	8.79	35.5	198	49	10.3
19X-3, 145–150	170.95	7.42	34.0	32.5	547	488	<1.3	58	7.10	984	9.82	32.3	206	54	9.3
22X-3, 145–150	199.75	7.37	29.4	32.0	544	484	<1.3	44	7.30	960	10.1	30.1	202	59	9.3
25X-3, 145–150	228.65	7.32	26.2	32.0	548	487	<1.3	35	7.00	973	10.2	28.7	221	67	9.0
28X-3, 145–150	257.45	7.35	22.6	32.0	547	485	<1.3	14	6.73	965	10.2	27.7	229	73	8.7
31X-3, 145–150	286.25	7.41	20.2	35.0	546	485	<1.3	16	6.13	1059	10.3	26.1	237	80	8.5
34X-3, 145–150	315.15	7.36	17.8	32.0	546	483	<1.3	19	5.81	1055	10.7	25.2	249	88	8.6
37X-3, 145–150	344.15	7.34	15.7	31.5	548	485	<1.3	11	5.52	1027	10.9	24.1	261	101	8.5
40X-3, 145–150	373.15	7.28	12.5	31.5	546	482	<1.3	6	4.77	1057	10.5	23.8	249	116	8.3
43X-3, 145–150	401.95	7.39	11.2	31.0	552	488	<1.3	5	4.70	1120	11.5	22.0	269	141	8.5

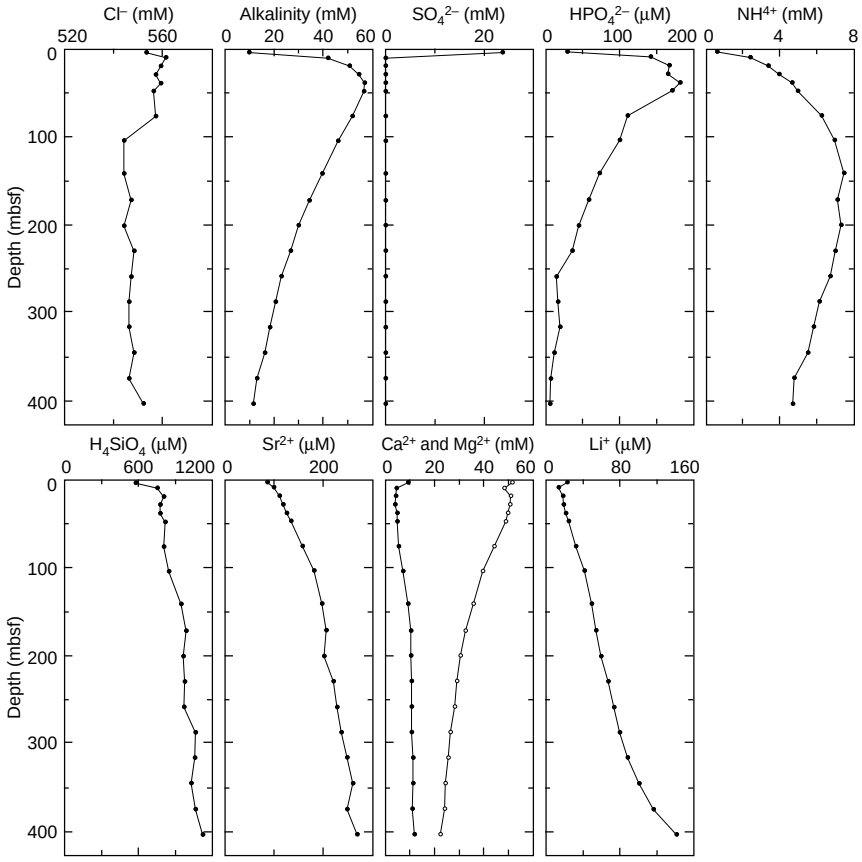

Figure 17. Interstitial water geochemical data, Site 1018. Solid circles = Ca, open circles = Mg.

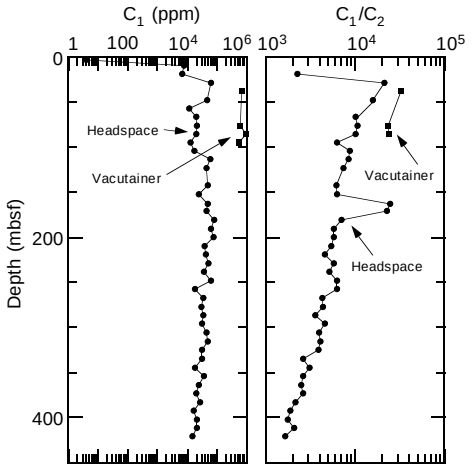

Figure 18. Depth variations of concentrations of methane (C_1) and methane/ethane (C_1/C_2) ratios obtained by the headspace and vacutainer techniques from Hole 1018A.

Table 16. Concentrations of methane (C_1), ethene ($C_{2=}$), ethane (C_2), and propane (C_3) obtained by the headspace and vacutainer techniques from Hole 1018A.

Core, section, interval (cm)	Depth (mbsf)	C_1 (ppm)	$C_{2=}$ (ppm)	C_2 (ppm)	C_3 (ppm)	C_1/C_2
Headspace						
167-1018A-						
1H-3, 0–5	3.03	4				
2H-4, 0–5	9.43	7,941				
3H-4, 0–5	18.93	6,815		3		2,272
4H-4, 0–5	28.43	63,366		3		21,122
6H-4, 0–5	47.43	47,622		3	4	15,874
7H-4, 0–5	56.93	11,848				
8H-4, 0–5	66.43	20,303		2	1	10,152
9H-4, 0–5	75.93	21,408		2	3	10,704
10H-4, 0–5	85.43	20,304		2	1	10,152
11X-4, 0–5	94.93	12,612		2	2	6,306
12X-4, 0–5	103.63	17,490		2	2	8,745
13X-4, 0–5	113.23	59,545		7	7	8,506
14X-4, 0–5	122.83	44,151		6	7	7,359
16X-3, 0–5	127.23	48,934		8	10	6,117
17X-4, 0–5	151.83	25,210		4	5	6,303
18X-5, 0–5	162.93	49,523		2	8	24,762
19X-4, 0–5	171.03	45,432		2	8	22,716
20X-4, 0–5	180.63	84,210	3	12	11	7,018
21X-4, 0–5	190.23	63,366	3	11	11	5,761
22X-4, 0–5	199.83	75,524	2	13	11	5,810
23X-4, 0–5	209.43	37,810		7	6	5,401
24X-4, 0–5	219.03	41,739		9	7	4,638
25X-4, 0–5	228.73	52,158		9	7	5,795
26X-4, 0–5	238.33	36,333		7	5	5,190
27X-4, 0–5	248.03	62,998		10	6	6,300
28X-4, 0–5	257.53	18,948		3		6,316
29X-4, 0–5	267.03	34,513		8	5	4,314
30X-4, 0–5	276.73	30,587		7	5	4,370
31X-4, 0–5	286.33	35,646		10	6	3,565
32X-4, 0–5	296.03	32,052		7	4	4,579
33X-4, 0–5	305.63	43,566		11	6	3,961
34X-4, 0–5	315.23	48,902		12	6	4,075
35X-4, 0–5	324.83	31,085		8	3	3,886
36X-4, 0–5	334.53	31,225	2	12	6	2,602
37X-4, 0–5	344.23	18,338		6	2	3,056
38X-4, 0–5	353.93	36,411	2	14	6	2,601
39X-4, 0–5	363.53	24,781		10	4	2,478
40X-4, 0–5	373.23	20,809		8	5	2,601
41X-4, 0–5	382.83	27,821		13	6	2,140
42X-4, 0–5	392.43	16,852	2	9	5	1,872
43X-4, 0–5	402.03	21,174	3	12	6	1,765
44X-4, 0–5	411.53	20,842		10	3	2,084
45X-4, 0–5	420.83	14,804		9	4	1,645
Vacutainer						
167-1018A-						
5H-4, 50–51	37.96	691,558		21	9	32,931
9H-4, 50–51	75.93	611,037		26	13	23,501
10H-4, 50–51	85.43	962,616		40	19	24,065
11H-4, 50–51	94.93	562,040				

Table 17. Concentrations of inorganic carbon, calcium carbonate, total carbon, total organic carbon, total nitrogen, and total sulfur in weight percent (wt%) in Hole 1018A.

Core, section, interval (cm)	Depth (mbsf)	Inorganic carbon (wt%)	$CaCO_3$ (wt%)	Total carbon (wt%)	Total organic carbon (wt%)	Total nitrogen (wt%)	Total sulfur (wt%)	Total organic carbon/ Total nitrogen
167-1018A-								
1H-1, 48–49	0.48	0.19	1.58	2.7	2.51	0.3	0.46	8.37
1H-2, 48–49	1.98	0.54	4.5	2.02	1.48	0.18	0.57	8.22
1H-3, 29–30	3.29	0.46	3.83	1.58	1.12	0.11	0.33	10.18
1H-4, 29–30	4.29	0.18	1.50	0.85	0.67	0.07	0.00	9.57
2H-1, 100–101	5.90	0.24	2.00	1.13	0.89	0.13	0.14	6.85
2H-2, 29–30	6.69	0.13	1.08	1.29	1.16	0.15	0.14	7.73
2H-3, 29–30	8.19	0.46	3.83	1.82	1.36	0.21	0.00	6.48
2H-4, 29–30	9.69	0.14	1.17	1.71	1.57	0.22	0.24	7.14
2H-5, 29–30	11.19	0.27	2.25	1.58	1.31	0.17	0.29	7.71
2H-6, 29–30	12.69	0.21	1.75	1.38	1.17	0.18	0.22	6.50

Only part of this table is produced here. The entire table appears on CD-ROM, back pocket, this volume.

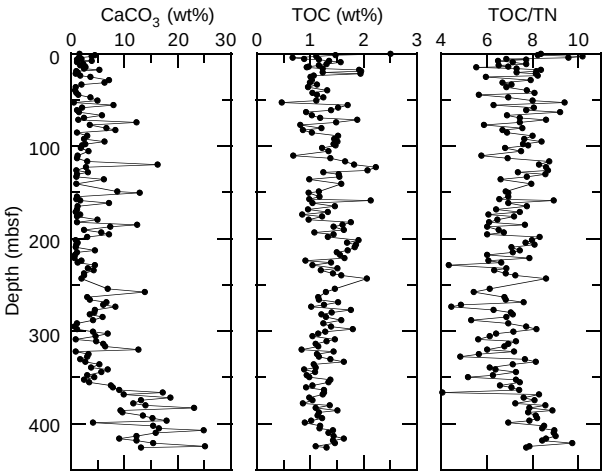

Figure 19. Depth variations of calcium carbonate and total organic carbon contents (TOC) and total organic carbon/total nitrogen (TOC/TN) in sediments of Hole 1018A.

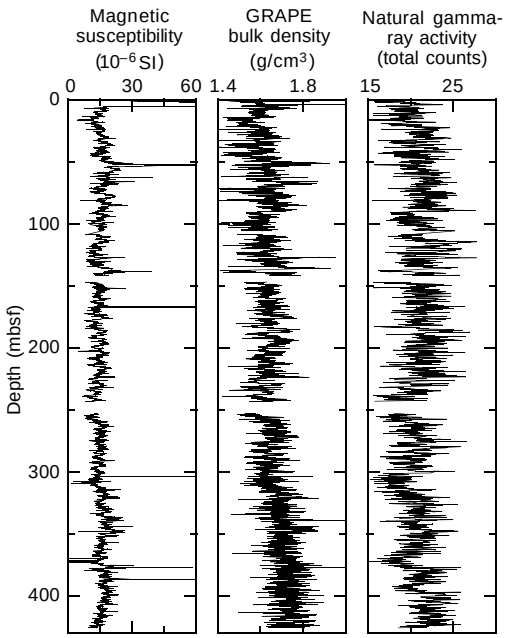

Figure 20. MST data from Hole 1018A.

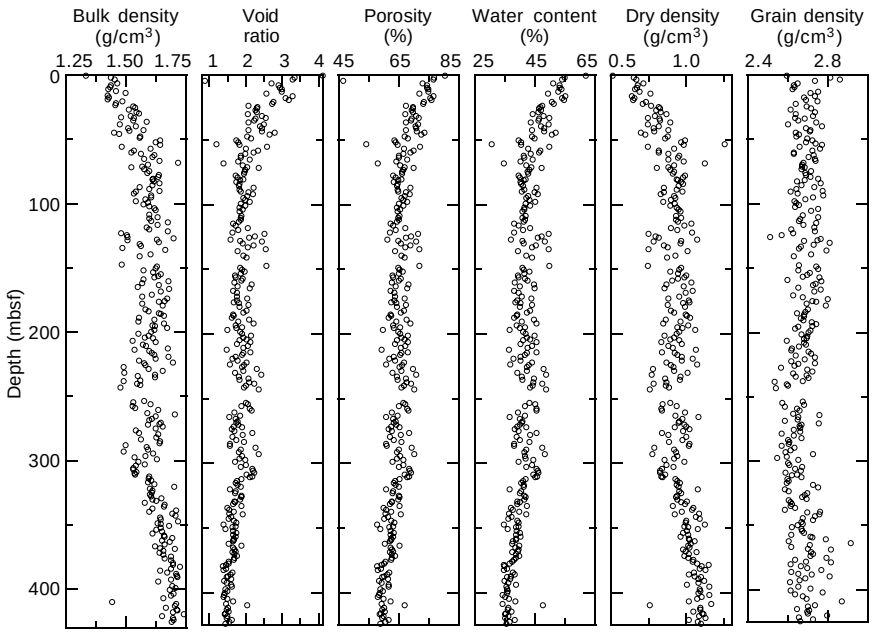

Figure 21. Index property data from Hole 1018A.

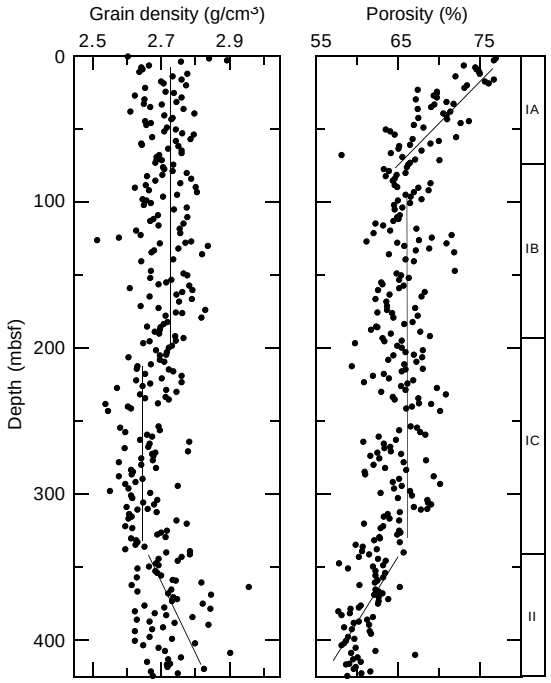

Figure 22. Grain density and porosity trends alongside lithostratigraphy from Hole 1018A.

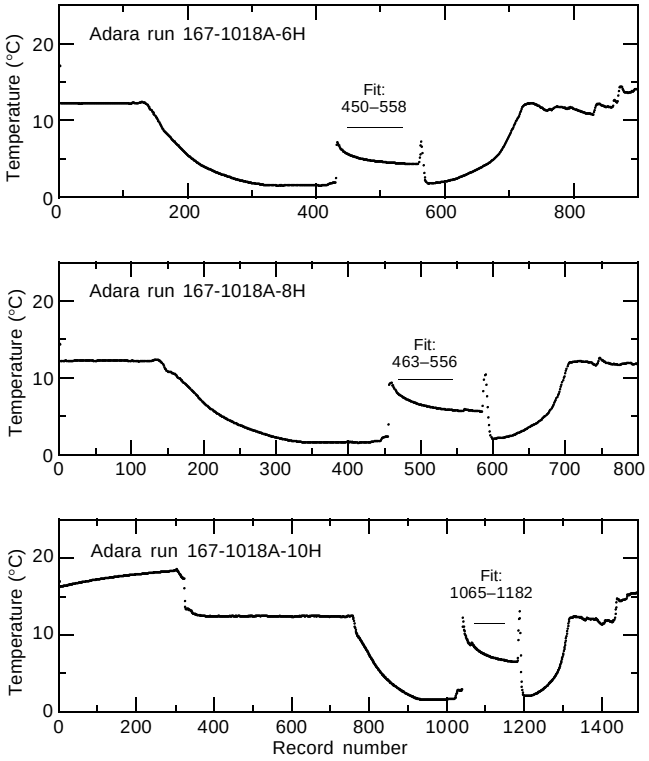

Figure 23. Hole 1018A downhole temperature vs. record number (5-s recording frequency) for each measurement run, showing the intervals fitted to determine the downhole temperature.

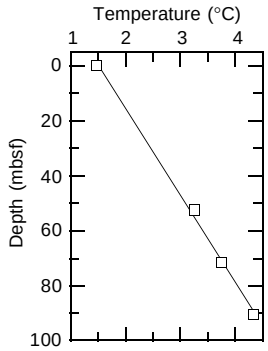

Figure 24. Downhole temperature gradient for Hole 1018A.

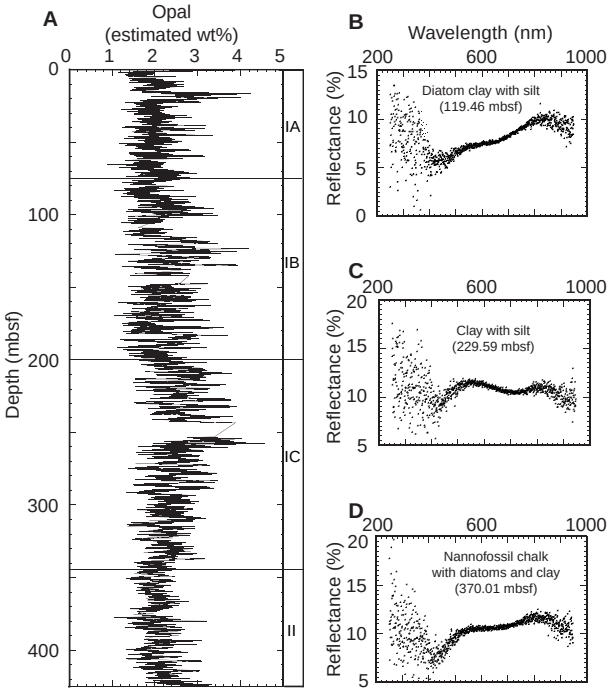

Figure 25. **A.** Predicted opal content for Hole 1018A based on site-survey core color reflectance and measured opal data. Characteristic reflectance spectra of (**B**) diatom clay with silt, (**C**) clay with silt, and (**D**) nannofossil chalk with diatoms and clay.

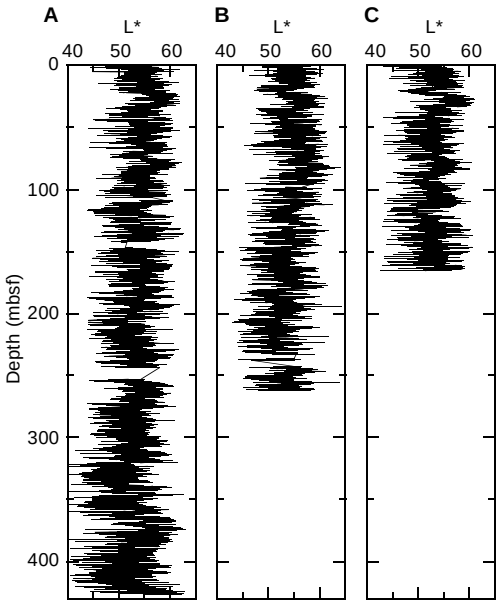

Figure 26. Digital color video data for CIELAB L* from Holes (**A**) 1018A, (**B**) 1018C, and (**C**) 1018D. Data were decimated at 2-cm intervals.

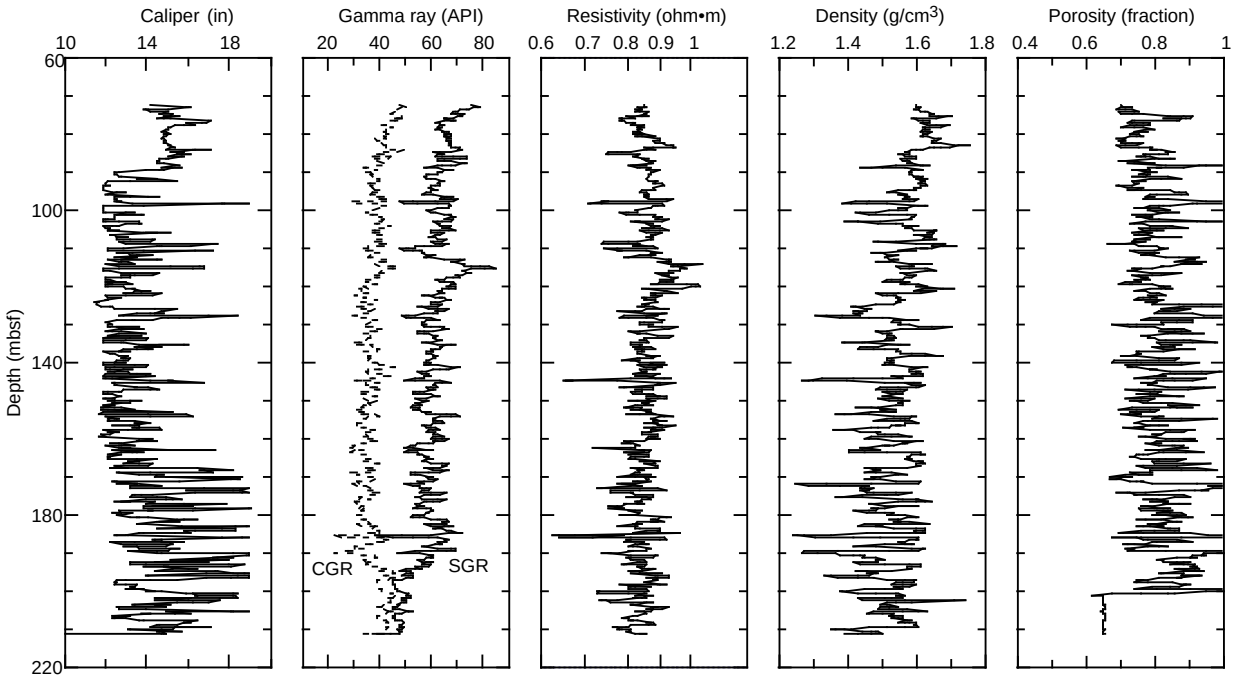

Figure 27. Downhole log data from the density-porosity combination tool string (pass 1). The very irregular caliper curve indicates poor borehole conditions. SGR = sum of all gamma-ray activity (K, U, Th); CGR = computed gamma-ray activity of K and Th, the silicate-bound elements.

Table 20. Downhole measurements at Hole 1018A.

Date, time	Description
May 25, 1996	
0000	Set pipe at 80 mbsf, wireline rig up, RIH density-porosity combination tool string, seas moderate (2-m swell).
0145	Tool string will not pass ledge at 222 mbsf. Wireline heave compensator on, start density-porosity pass 1 (227–70 mbsf); 300 m/hr, continue logging to mudline, and POOH.
0330	Rig down density-porosity tool string, conduct second wiper trip to TD (426 mbsf), set base of pipe to 234 mbsf.
0830	Rig up density-porosity combination tool string, RIH.
1100	Tool string will not pass ledge at 342 mbsf. Begin pass 2 (342–234 mbsf) at 300 m/hr.
1145	End pass 2, POOH, rig down density-porosity tool string, conclude logging operations.

Note: RIH = run in hole, TD = total depth, POOH = pull out of hole.

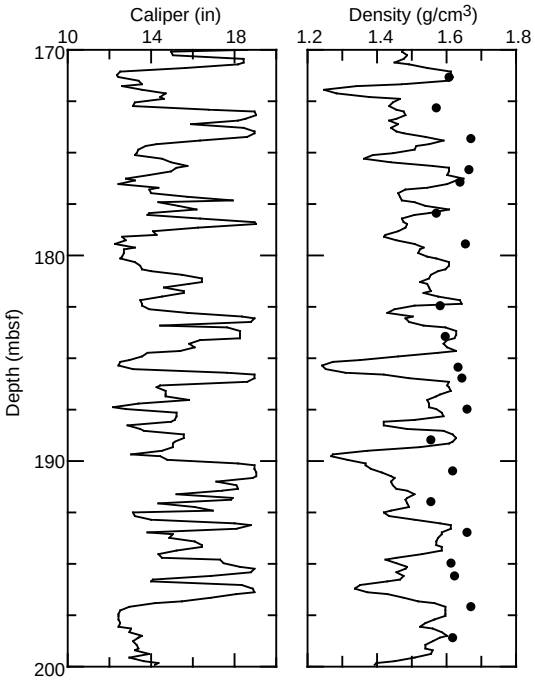

Figure 28. Detail of the caliper measurement of hole diameter and the effect of borehole washouts on log density measurement. Core index property density data are shown as solid dots.

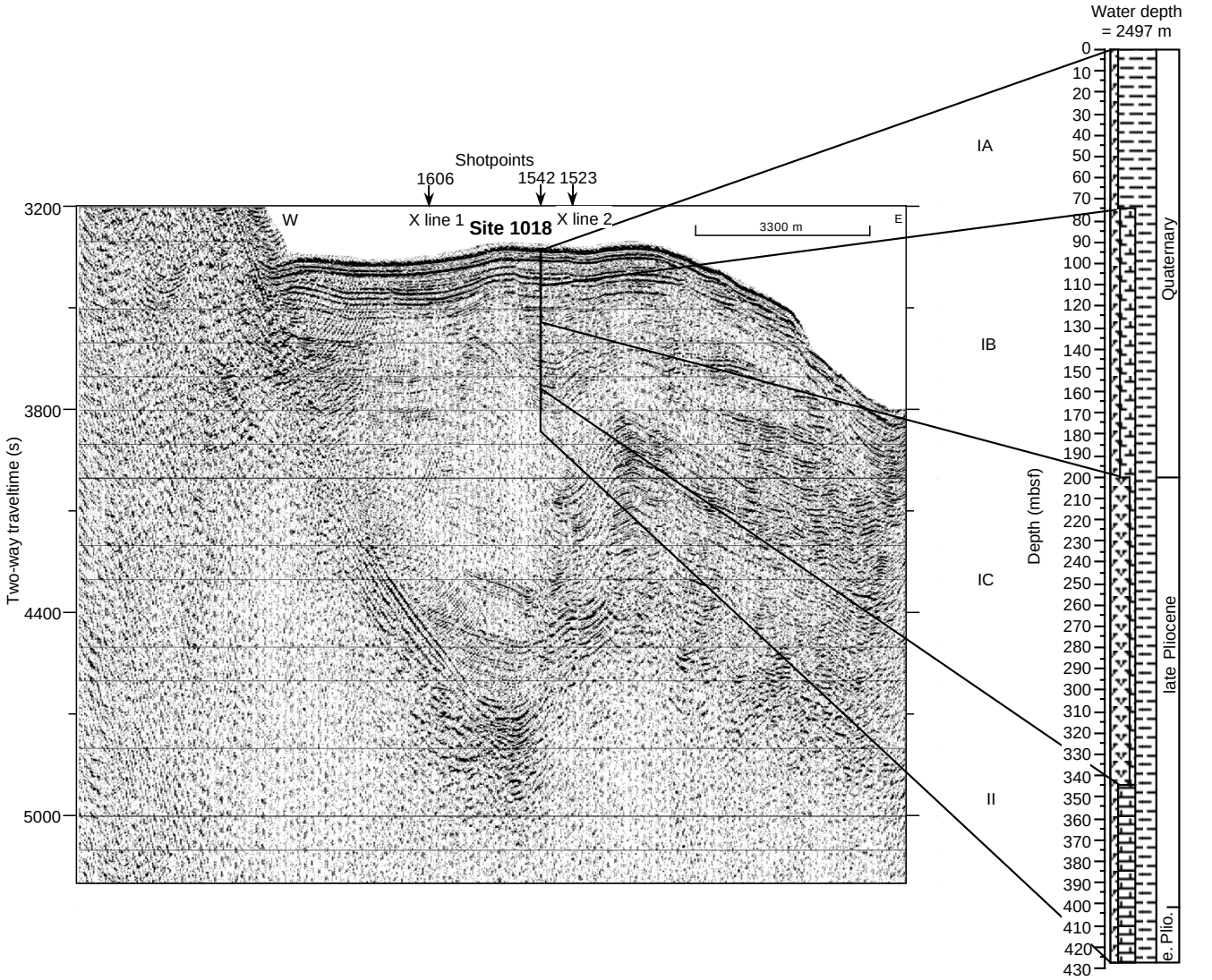

Figure 29. Comparison of the lithostratigraphic column at Site 1018 and a seismic reflection profile through the site (Line EW9504 CA8-3; Lyle et al., 1995b). Ties are calculated from an estimated velocity profile. On y-axis, (s) = milliseconds.

SHORE-BASED LOG PROCESSING

HOLE 1018A

Bottom felt: 2488.6 mbrf (used for depth shift to seafloor)
Total penetration: 426.9 mbsf
Total core recovered: 426.9 m (100%)

Logging Runs

Logging string 1: DIT/HLDT/APS/HNGS (upper and lower section)

Wireline heave compensator was used to counter ship heave.

Bottom-Hole Assembly

The following bottom-hole assembly depths are as they appear on the logs after depth shift to the seafloor. As such, there might be a discrepancy with the original depths given by the drillers onboard. Possible reasons for depth discrepancies are ship heave, use of wireline heave compensator, and drill string and/or wireline stretch.

DIT/HLDT/APS/HNGS: Bottom-hole assembly at ~53 mbsf (upper section).

DIT/HLDT/APS/HNGS: Bottom-hole assembly at ~238 mbsf (lower section).

Processing

Depth shift: Because of lack of correlation in the limited overlapping section between the upper and lower section of the logged interval, no differential depth shift has been performed. Original logs have only been depth shifted to the seafloor (–2488.6 m).

Gamma-ray and environmental corrections: HNGS data from the DIT/HLDT/APS/HNGS tool string were corrected in real-time during the recording.

Quality Control

Borehole conditions at Hole 1018A were extremely poor, the hole being affected by large washouts. In the lower section of the logged interval, the caliper closed at 270–286 mbsf because of tool sticking problems; this resulted in suspiciously lower density readings.

Data recorded through bottom-hole assembly, such as the HNGS data above 53 mbsf (upper section) and 238 mbsf (upper section) should be used qualitatively only because of the attenuation on the incoming signal.

Hole diameter was recorded by the hydraulic caliper on the HLDT tool (CALI).

Note: Details of standard shore-based processing procedures are found in the "Explanatory Notes" chapter, this volume. For further information about the logs, please contact:

Cristina Broglia
Phone: 914-365-8343
Fax: 914-365-3182
E-mail: chris@ldeo.columbia.edu

Zhiping Tu
Phone: 914-365-8336
Fax: 914-365-3182
E-mail: ztu@ldeo.columbia.edu

Hole 1018A: Natural Gamma Ray-Density-Porosity Logging Data

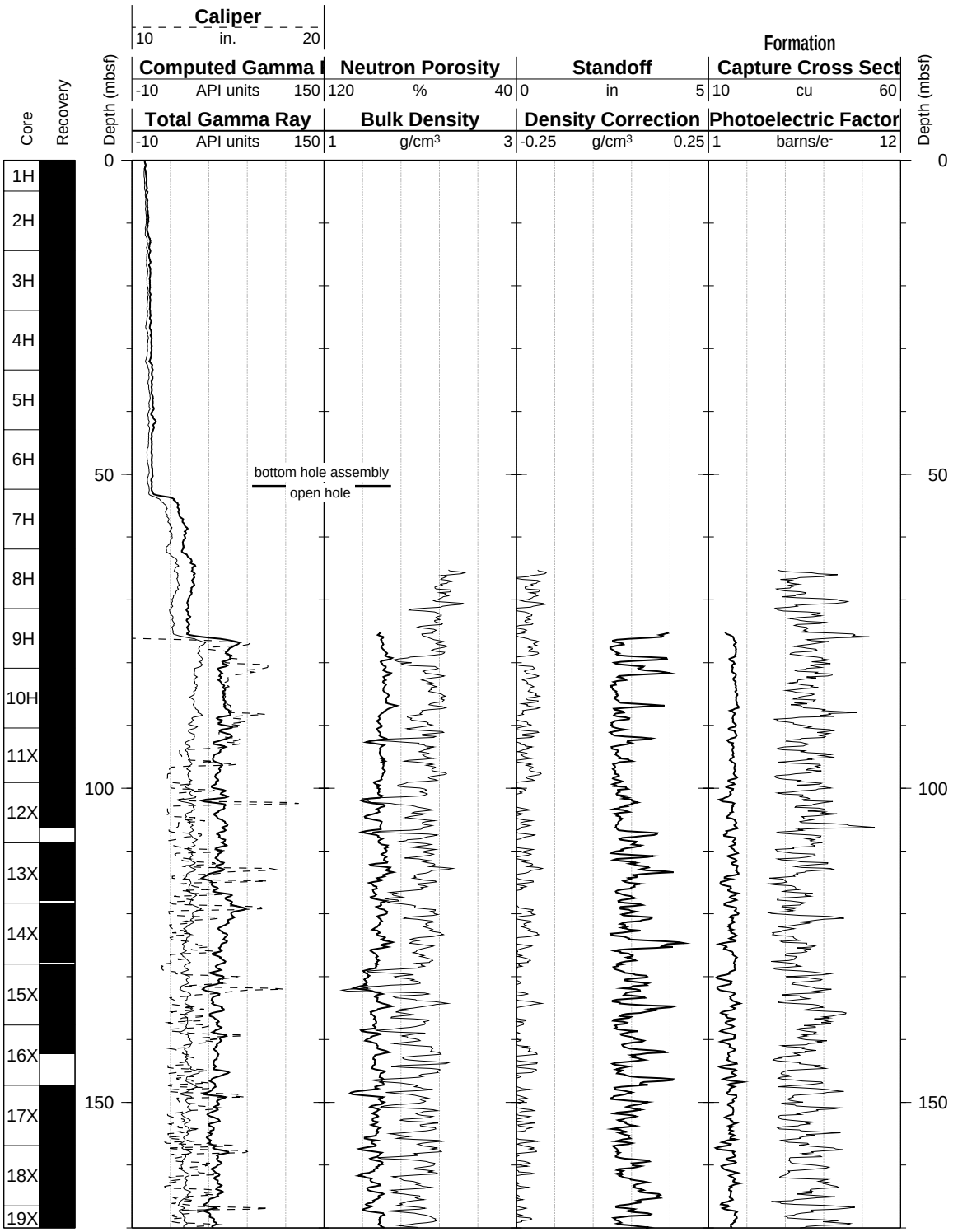

Hole 1018A: Natural Gamma Ray-Density-Porosity Logging Data (cont.)

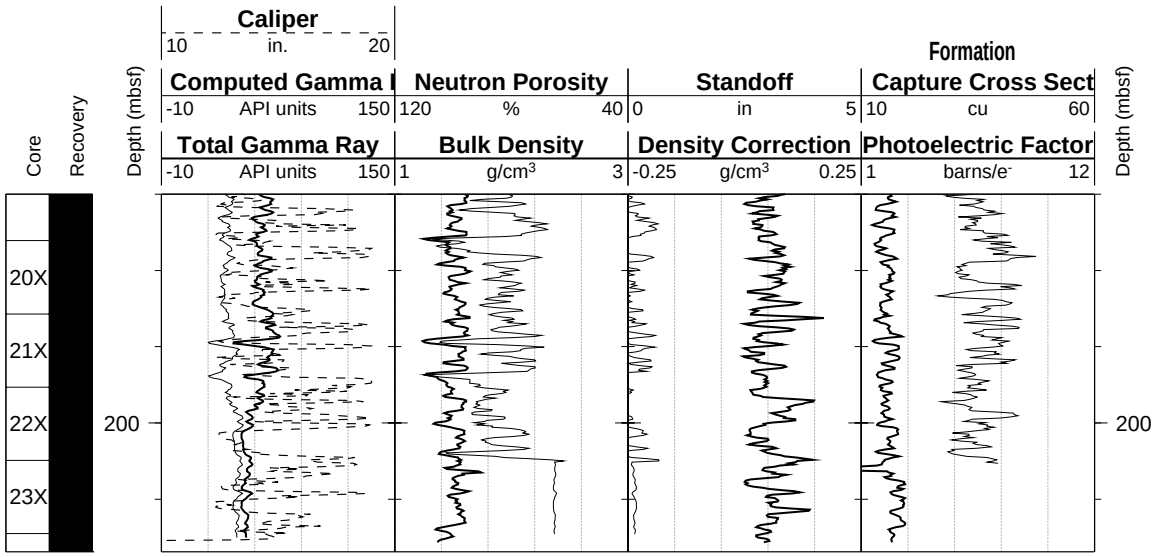

Hole 1018A: Natural Gamma Ray-Resistivity Logging Data

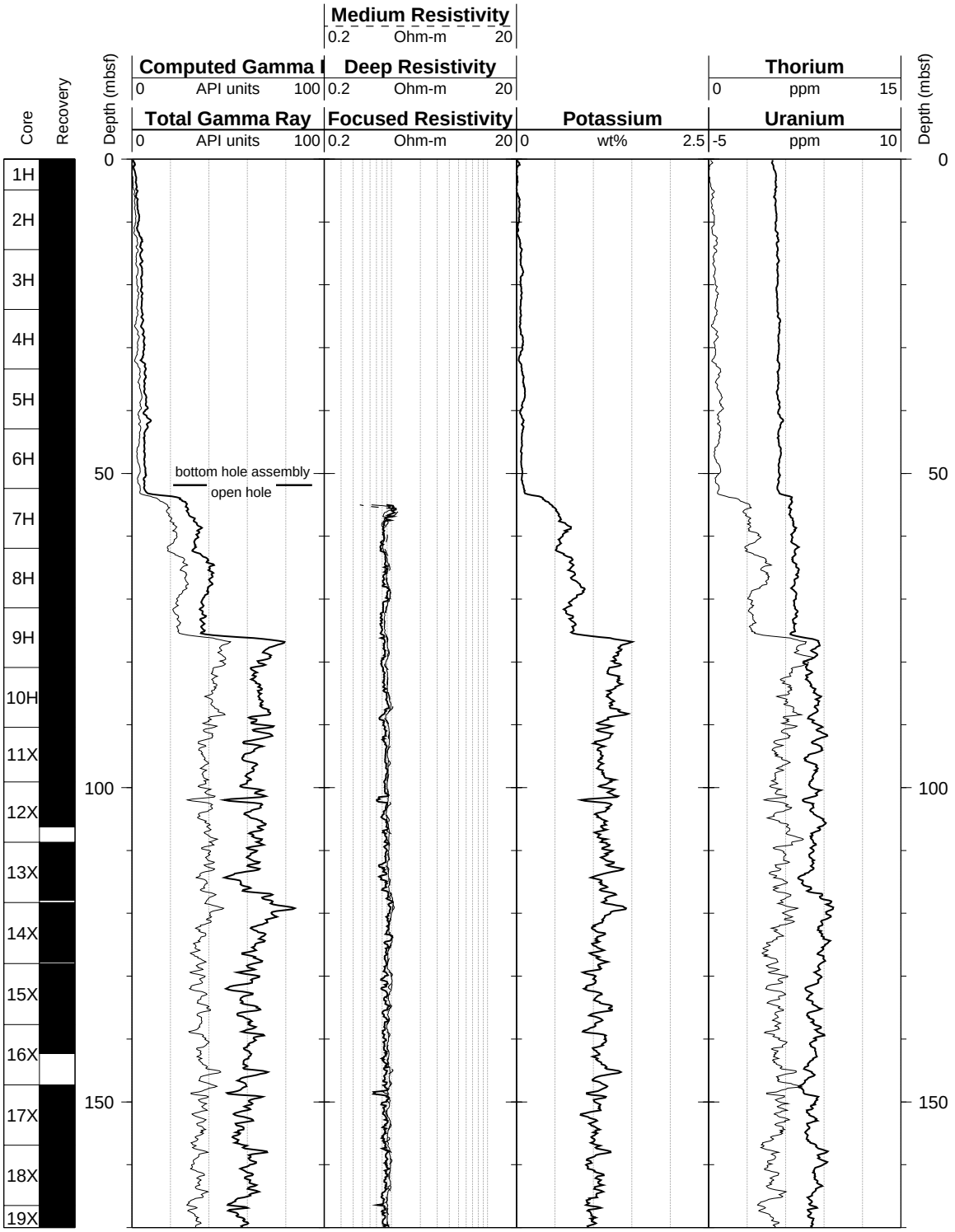

Hole 1018A: Natural Gamma Ray-Resistivity Logging Data (cont.)

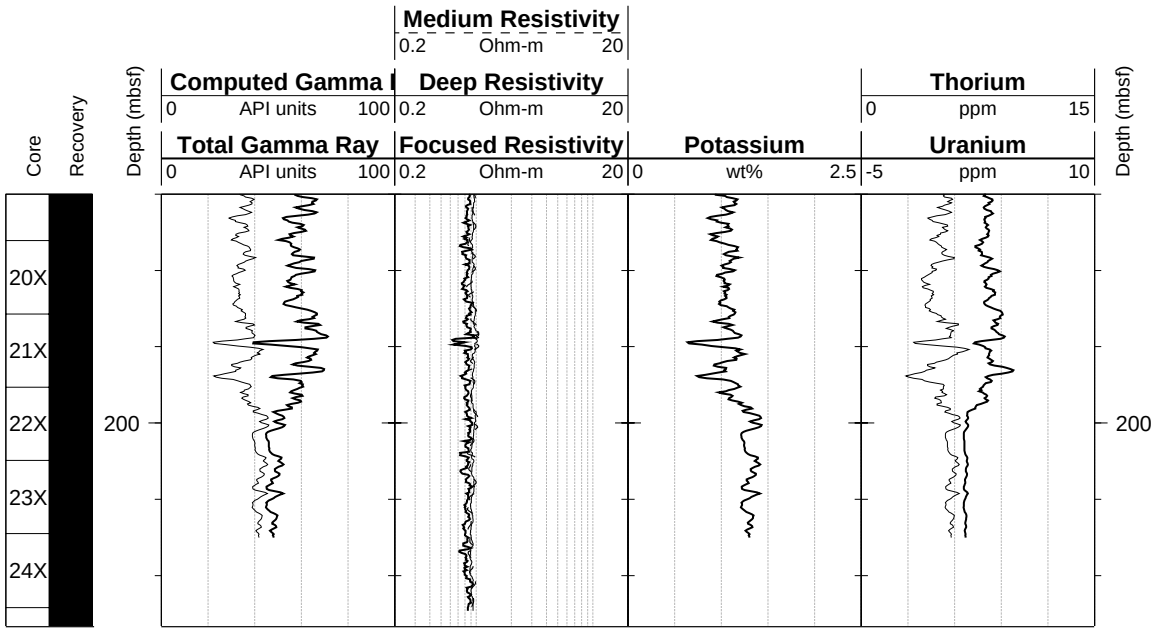

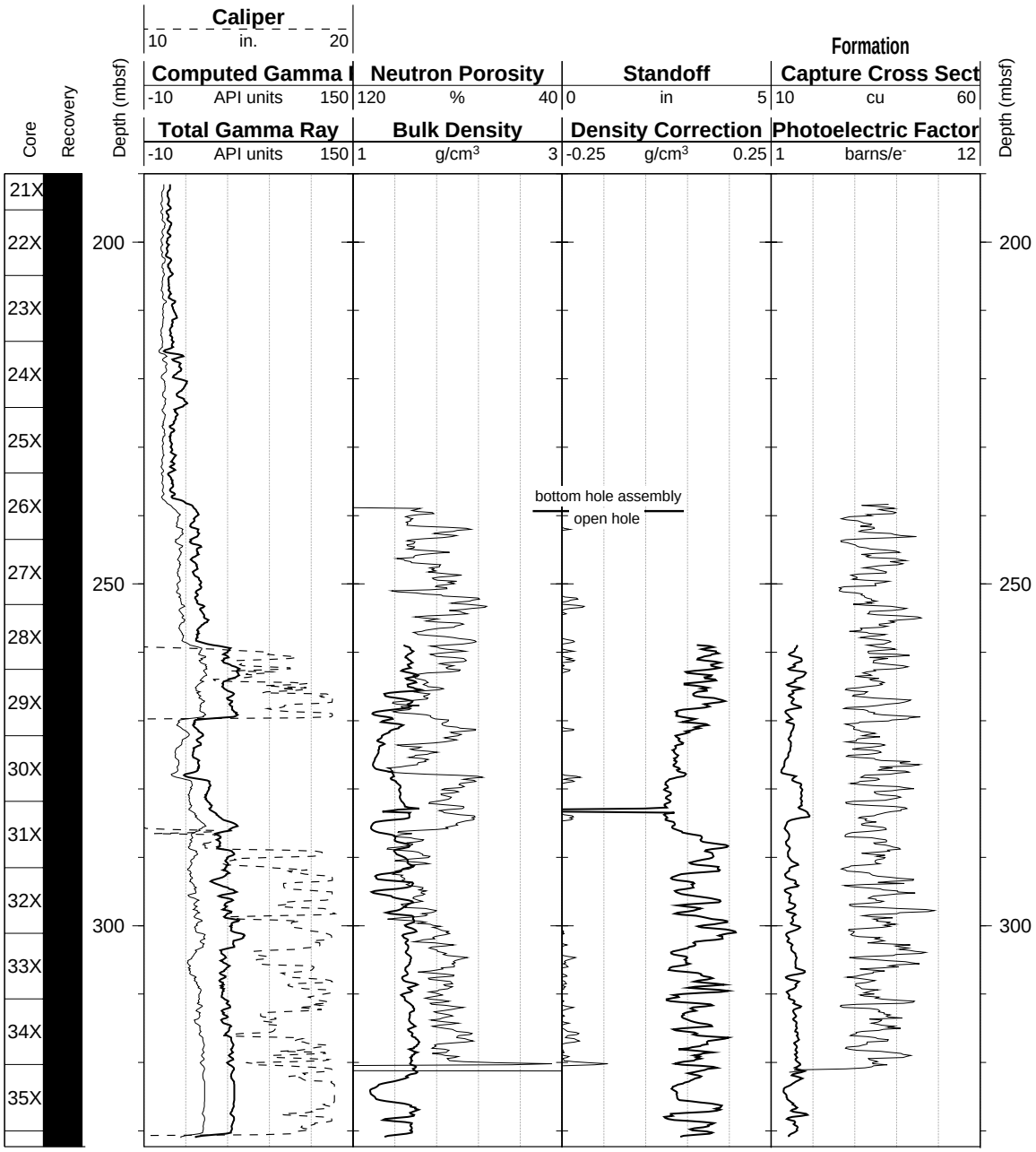
Caliper
10 in. 20
Computed Gamma I
-10 API units 150
Neutron Porosity
120 % 40
Standoff
0 in 5
Capture Cross Sect
10 cu 60
Total Gamma Ray
-10 API units 150
Bulk Density
1 g/cm3 3
Density Correction
-0.25 g/cm3 0.25
Photoelectric Factor
1 barns/e- 12
Formation
Core
Recovery
Depth (mbsf)
Depth (mbsf)
21X
22X
23X
24X
25X
26X
27X
28X
29X
30X
31X
32X
33X
34X
35X
200
250
300
bottom hole assembly
open hole

Hole 1018A: Natural Gamma Ray-Resistivity Logging Data

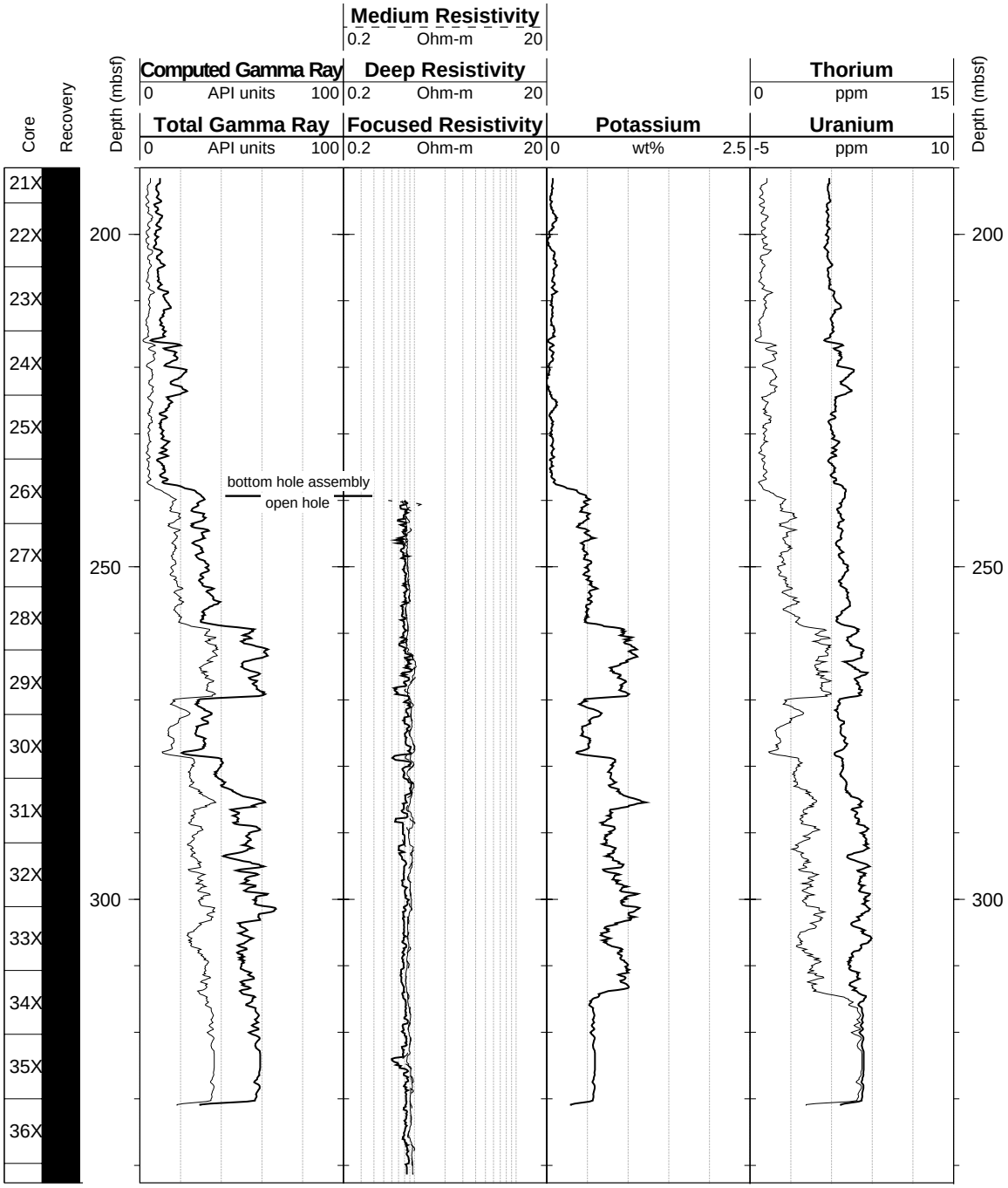

Previous Chapter Table of Contents Next Chapter